Published March 9, 2009

CX_3CR1^+ $CD115^+$ $CD135^+$ common macrophage/DC precursors and the role of CX_3CR1 in their response to inflammation

Cedric Auffray,[1] Darin K. Fogg,[1] Emilie Narni-Mancinelli,[2] Brigitte Senechal,[1] Celine Trouillet,[1,3] Noah Saederup,[4] Julia Leemput,[5] Karine Bigot,[5] Laura Campisi,[2] Marc Abitbol,[5] Thierry Molina,[1] Israel Charo,[4] David A. Hume,[6] Ana Cumano,[7] Gregoire Lauvau,[2] and Frederic Geissmann[1,3]

[1]Laboratory of Biology of the Mononuclear Phagocyte System, Institut National de la Santé et de la Recherche Médicale (INSERM) U838, Université Paris-Descartes, 75015 Paris, France
[2]INSERM U924, Université de Nice-Sophia Antipolis, 06560 Valbonne, France
[3]Centre for Inflammation Biology, Division of Immunity, Infection, and Inflammatory Diseases, King's College London, SE1 9RT London, England, UK
[4]Gladstone Institute of Cardiovascular Disease, University of California, San Francisco, San Francisco, CA 94158
[5]Centre d'etude et de recherche therapeutique en ophtalmologie, Université Paris-Descartes, 75015 Paris, France
[6]The Roslin Institute and Royal (Dick) School of Veterinary Studies, University of Edinburgh, EH25 9PS Roslin, Scotland, UK
[7]INSERM U668, Unité de Développement des Lymphocytes, Institut Pasteur, 75015 Paris, France

CX_3CR1 expression is associated with the commitment of $CSF\text{-}1R^+$ myeloid precursors to the macrophage/dendritic cell (DC) lineage. However, the relationship of the $CSF\text{-}1R^+$ CX_3CR1^+ macrophage/DC precursor (MDP) with other DC precursors and the role of CX_3CR1 in macrophage and DC development remain unclear. We show that MDPs give rise to conventional DCs (cDCs), plasmacytoid DCs (PDCs), and monocytes, including $Gr1^+$ inflammatory monocytes that differentiate into TipDCs during infection. CX_3CR1 deficiency selectively impairs the recruitment of blood $Gr1^+$ monocytes in the spleen after transfer and during acute *Listeria monocytogenes* infection but does not affect the development of monocytes, cDCs, and PDCs.

CORRESPONDENCE
Frederic Geissmann:
frederic.geissmann@kcl.ac.uk

Abbreviations used: cDC, conventional DC; CDP, common DC precursor; GMP, granulocyte-macrophage progenitors; iNOS, inductible nitric oxide synthase; *Lm*, *Listeria monocytogenes*; MDP, macrophage/DC precursor; PDC, plasmacytoid DC; PI, propidium iodide; ROI, reactive oxygen intermediate.

Monocytes, macrophages, and DCs form networks of phagocytic cells throughout most tissues, the development of which are dependent on the CSF-1 receptor (csf1r, also known as CD115, c-fms, and M-CSF receptor) (1, 2). These cells, which are sometimes referred to as the mononuclear phagocyte system, play major roles in development, scavenging, inflammation, and antipathogen defenses (3, 4). They are highly heterogeneous in phenotype, tissue distribution, and function (3, 5, 6). Considerable attention is currently focused on the characterization of their progenitors and precursors, the signals driving their development in the BM, their migration to tissues, and their homeostasis in peripheral tissues. CSF-1R and its two known ligands, M-CSF and IL34 (7), are critical for the development of this lineage because M-CSF–deficient mice (op/op and $csf1^{-/-}$) have a milder phenotype than the Csf1r-deficient mice (8). Other cytokines, such as GM-CSF, FLT3, LT-$\alpha1\beta2$ (LT-α) (9–15), and chemokines (16, 17) have also been shown to control the development and homeostasis of the macrophage and DC networks.

Cellular cloning and transplantation studies have shown that many macrophage subsets, most of the conventional DCs (cDCs) in the secondary lymphoid organs of mice, and at least a fraction of the DCs in the mouse thymus probably originate from myeloid progenitors (18–20).

C. Auffray, D.K. Fogg, and E. Narni-Mancinelli contributed equally to this paper.

The Rockefeller University Press $30.00
J. Exp. Med. Vol. 206 No. 3 595-606
www.jem.org/cgi/doi/10.1084/jem.20081385

Published March 9, 2009

Granulocyte-macrophage progenitors (GMPs [reference 21]) include a clonogenic BM macrophage/DC precursor (MDP) that gives rise to spleen cDCs (both the CD11c$^+$ CD8α^+ CD11b$^-$ and CD11c$^+$ CD8α^- CD11b$^+$ subsets) directly, with no monocytic intermediate, and to monocytes and macrophages (9, 22, 23). The MDP has no significant granulocytic potential, and initial studies failed to detect a plasmacytoid DC (PDC) potential (9, 22). Another precursor, common DC precursor (CDP), was recently shown to give rise to cDCs and PDCs but not to monocytes, and it did not respond to CSF-1 (24, 25). This result was interpreted as indicating the existence of two pathways for cDC generation. However, MDPs and CDPs are both included in the CD115$^+$ lin$^-$ fraction of BM progenitors (9) and could represent different stages of differentiation along the same pathway. It is also possible that differences in differentiation potential between these cells reported by different groups may reflect differences in experimental protocols rather than intrinsic properties of the cells.

The chemokine receptor and adhesion molecule CX_3CR1 is not expressed on early hematopoietic progenitors and is first detected on MDPs. CX_3CR1 is therefore associated with the commitment of myeloid progenitors to the monocyte/macrophage/DC lineage (22). However, its role in the development and homeostasis of cells of the mononuclear phagocyte system remains unknown.

In this paper, we therefore reevaluated the differentiation potential of the MDP and the possible roles of CX_3CR1 in the differentiation of mononuclear phagocytes in mice using adoptive transfer and disease models. We found that MDPs can give rise to PDCs, as well as to cDCs and monocytes, after adoptive transfer and that MDPs and CDPs share a similar surface phenotype (Lin$^-$ IL7Ra$^-$ CD117^{int} CD135$^+$ CD115$^+$ CX_3CR1^+). The use of AFS98, an antibody designed to block CSF-1 binding to its receptor CD115, and CSF-1–dependent proliferation (26–28) to purify MDP did not impair the ability of MDP to give rise to monocytes, cDCs, or PDCs in vivo. Because MDP can give rise to PDCs, cDCs, and monocytes/macrophages, whereas CDP only give rise to PDCs and cDCs (24, 25), MDP appears to exhibit a broader differentiation potential than CDP and may represent an earlier precursor. CX_3CR1 deficiency decreased the recruitment into the spleen of CD115$^+$ Gr1$^+$ monocytes (TipDC precursors) after irradiation and during acute *Listeria monocytogenes* infection and decreased the efficiency of bacterial clearance but did not affect the development of cDCs or PDCs. The results from this study, therefore, clarify the family tree of mononuclear phagocytes and uncover the role of CX_3CR1 in Gr1$^+$ monocyte recruitment to the spleen during inflammation and infection.

RESULTS

MDPs and CDPs are phenotypically overlapping cell populations in mouse BM

Expression of the chemokine receptor CX_3CR1 in GMPs (Lineage$^-$ CD117$^+$ Sca1$^-$ IL7Rα^- CD34$^+$ CD16/32$^+$ BM cells) (21) characterizes the MDP (22) and is thus associated with the commitment of myeloid progenitors toward the macrophage/DC lineage. The MDP is also characterized by a low expression of CD117 (c-kit, the receptor for stem cell factor), as compared with GMPs and CMPs (22), and expression of functional CSF-1R (CD115) and FLT3 (CD135) (9, 22). More recently, a precursor common to cDCs and PDCs (CDP) was reported and proposed to be distinct from the MDPs because the CDP gave rise to both cDCs and PDCs but not to monocytes/macrophages, whereas the MDPs give rise to cDCs and monocytes/macrophages but not to PDCs (24, 25). We performed an analysis of mouse BM Lin$^-$ precursors by flow cytometry (Fig. 1 a), and the results indicated that most CDPs expressed CX_3CR1 at levels similar to its level of expression on MDPs, and that most MDPs expressed both CSF-1R/CD115 and CD135 at levels similar to their expression on CDPs (Fig. 1). These data confirm the data from Waskow et al. (9) suggesting that MDPs and CDPs had an overlapping phenotype in the BM, and we therefore sought to reevaluate the differentiation potential of MDPs.

MDPs give rise to monocytes, cDCs, and PDCs

Initial studies failed to identify PDCs in the progeny of MDPs after in vivo transfer into C57BL/6 mice (9, 22, 23). However, PDCs in spleen express a CSF-1R-EGFP transgene (2), and we observed that PDCs also expressed CX_3CR1 (Fig. S1, available at http://www.jem.org/cgi/content/full/jem.20081385/DC1) and that MDP gave rise to a population of CD11b$^-$ CD11c^{int} CX_3CR1^+ splenocytes that are distinct from cDCs and monocyte/macrophages and may correspond to PDCs after in vivo transfer into irradiated hosts (Fig. S1). In addition, the availability of PDCA1 antibody now permits a better phenotypic definition of PDC (24, 25). We thus investigated the differentiation potential in vivo of MDP, purified as previously described (Fig. S2) (22), after i.v. adoptive transfer. BM MDP from $CX_3CR1^{gfp/+}$ of the *Cd45.1/Cd45.2* genotypes was injected i.v. into *Cd45.2*-irradiated hosts, and splenocytes were analyzed by flow cytometry 6–7 d after transfer. Results indicated that MDP gave rise to donor-derived PDCA1$^+$ CD11c^{int} CD11b$^-$ CX_3CR1^+ PDC, as well as to CD11c^{high} CD11b$^-$ CX_3CR1^- and CD11c^{high} CD11b$^+$ CX_3CR1^+ cDC and to CD11b$^+$ CD11c$^-$ CX_3CR1^+ monocytes (Fig. 2, a–c). As expected, the frequency of donor-derived PDCs and monocytes in the spleen was 2–3-fold lower than that of CD11b$^+$ and CD11b$^-$ cDCs (Fig. 2 c). However, CD11b$^-$ PDCs were easily distinguishable from CD11b$^-$ cDCs by their expression of CX_3CR1 and PDCA1 and their low expression of CD11c (Fig. 2, a and b). MDP-derived CD11b$^+$ CD11c$^-$ monocytes expressed high levels of CX_3CR1 (Fig. 2 a), which unambiguously distinguished them from granulocytes which do not express CX_3CR1 (29).

Because the anti-CD115 antibody (AFS98) used to purify CDP (25), and MDP in one study (9), was originally screened for its ability to block the binding of CSF-1 to its receptor (26–28, 30, 31), we investigated whether labeling of MDPs with AFS98 would affect the differentiation of MDPs in our experimental model. We observed that, in vitro, the cloning

Published March 9, 2009

efficiency of single MDP seeded into 96-well plates in the presence of CSF-1, as well as the size of colonies, was reduced when AFS98 was added to the antibody cocktail used for cell sorting (Fig. S3, available at http://www.jem.org/cgi/content/full/jem.20081385/DC1). However, addition of AFS98 to the antibody cocktail used for cell sorting did not affect the differentiation potential of MDP in vivo (Fig. 2 c).

These data indicate that MDP and CDP share expression of CX_3CR1, CD115, and FLT3 and have an otherwise overlapping phenotype in the BM, whereas MDP appears to have a broader differentiation potential than CDP after adoptive transfer in vivo because MDP gave rise to both DCs (PDCs and cDCs) and monocyte/macrophages. It is of note that addition of AFS98 to the antibody cocktail used for cell sorting decreased the proliferative response of MDP to CSF-1 in vitro but did not affect their differentiation in to DCs or monocytes in vivo.

CX_3CR1-deficient MDPs have a decreased potential to give rise to spleen monocytes

Because expression of CX_3CR1 is associated with the commitment of myeloid progenitors to the monocyte/macrophage/DC lineage, we investigated the role of CX_3CR1 in the homeostasis of this lineage. The number of MDPs in the BM was not affected by CX_3CR1 deficiency (Fig. 3 a) and, on average, 6.5×10^4 MDPs were recovered per femur from *Cx3cr1*$^{+/-}$ and *Cx3cr1*$^{-/-}$ mice, suggesting that CX_3CR1 is dispensable for MDP development in the BM. We thus investigated the role of CX_3CR1 in DC and monocyte development from MDP by studying the fate of MDP in competitive adoptive transfer, in which 10^4 MDP from each of two different donors of the *Cd45.2* and *Cd45.2/Cd45.1* genotype were coinjected i.v. into a *Cd45.1* congenic recipient (Fig. 3 b). When both donor mice were of the *Cx3cr1*$^{+/-}$ genotype, CD45.2 and CD45.2/CD45.1 MDPs contributed equally to cDCs, PDCs, and CD11b$^+$ CD11c$^-$ monocytes (Fig. 3, b and c). When CD45.2 MDPS were of the *Cx3cr1*$^{-/-}$ genotype and CD45.2/CD45.1 MDPs were of the *Cx3cr1*$^{+/-}$ genotype, they contributed equally to spleen DCs and PDCs (Fig. 3, b and d). However, CX_3CR1-deficient MDP generated spleen CD11b$^+$ CD11c$^-$ cells with an efficiency of one fifth to one tenth that of the control (Fig. 3, b and d). MDP-derived CD11b$^+$ CD11c$^-$ splenocytes were negative for NK1.1, CD3, CD19, and Ly6G and expressed high levels of CX_3CR1 and intermediate levels of F4/80, and most of these cells expressed Gr1 (Fig. 3 e). These characteristics are similar to those of CD115$^+$ Gr1$^+$ blood monocytes (29) and of spleen monocytes, as recently described by Nahrendorf et al. (32). Thus, we concluded that CX_3CR1 may be selectively involved in the development, recruitment, proliferation, and/or survival of CD11b$^+$ CD11c$^-$ monocytes in the spleen.

CX_3CR1 is important for the recruitment of blood Gr1$^+$ monocytes to the spleen during infection and for the clearance of *Lm* in mice

The only known ligand of CX_3CR1 is the transmembrane chemokine fractalkine/CX_3CL1, which is expressed in neurons, endothelial cells, and DCs (33–37). CX_3CR1 is involved in the adhesion of leukocytes, including monocytes in particular, to endothelial cells (38–42) and in the migration of microglial cells (43). Fractalkine is expressed in the T cell areas of lymph nodes (37). PCR and in situ hybridization experiments indicated that CX_3CL1 was also expressed in the spleen (Fig. 4, a and b; and Fig. S4, available at http://www.jem.org/cgi/content/full/jem.20081385/DC1). Spleen CX_3CL1-producing cells were located at the periphery of the B cell follicle,

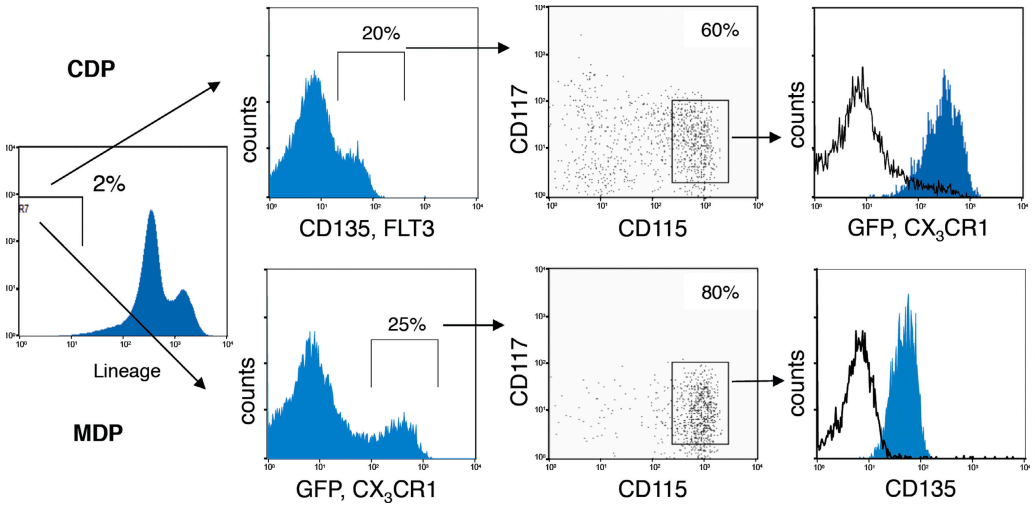

Figure 1. MDP and CDP share a similar phenotype. BM cells from *Cx3cr1*$^{gfp/+}$ reporter mice were labeled with antibodies against lineage markers (CD11c, CD11b, NK1.1, CD3, Ter119, CD19, and Gr1), ckit (CD117), FLT3 (CD135), and CSF-1-R (CD115) and analyzed by FACS. CDP and MDP are overlapping populations; lineage$^-$ CD117^{low} CD135$^+$ CD115$^+$ cells (CDP) express CX_3CR1 (gfp), whereas CD117^{int} CX_3CR1 CD115$^+$ cells (MDP) express CD135. Results are representative of >10 experiments.

Published March 9, 2009

which correspond to the marginal zone/T cell area (Fig. 4, a and b). The precise identification of CX_3CL1-expressing cells in the spleen will require the availability of specific antibodies; however, localization of *Cx3cl1* messenger RNA is compatible with the expression of CX_3CL1 in the marginal zone/T cell area of the spleen and, thus, with a role of CX_3CL1 in the recruitment of blood monocytes.

We tested the role of CX_3CR1 for the recruitment of monocytes in the spleen by adoptive transfer of monocytes and during infection with *Lm*. Short-term competitive transfer of BM monocytes from donors of *Cd45.2* and *Cd45.2/Cd45.1* genotype into irradiated *Cd45.1* congenic recipients indicated that CX_3CR1-deficient monocytes were only one tenth as efficient as control monocytes at accumulating in the spleen (Fig. 4 c). During *Lm* infection in CX_3CR1-deficient BALB/c mice, the number of monocytes was increased in the blood, whereas the number of monocytes in the spleen was decreased in comparison with controls (Fig. 4 d). A similar phenomenon was observed in C57BL/6 mice (Fig. 5, e and f) both for high (3×10^5 *Lm*; Fig. 4 e) and low (7×10^3 *Lm*; Fig. 5 f) numbers of bacteria. To investigate whether the proliferation of blood monocytes in the spleen of *Lm*-infected mice was involved in their accumulation in the spleen, monocytes from the BM and spleen of infected mice at 16 and 48 h after infection were isolated by flow cytometry and analyzed for DNA content using propidium iodide (PI) staining (Fig. 4 g and Fig. S5, available at http://www.jem.org/cgi/content/full/jem.20081385/DC1). Results indicated that BM monocytes, but not spleen monocytes, actively proliferate at 16 and 48 h

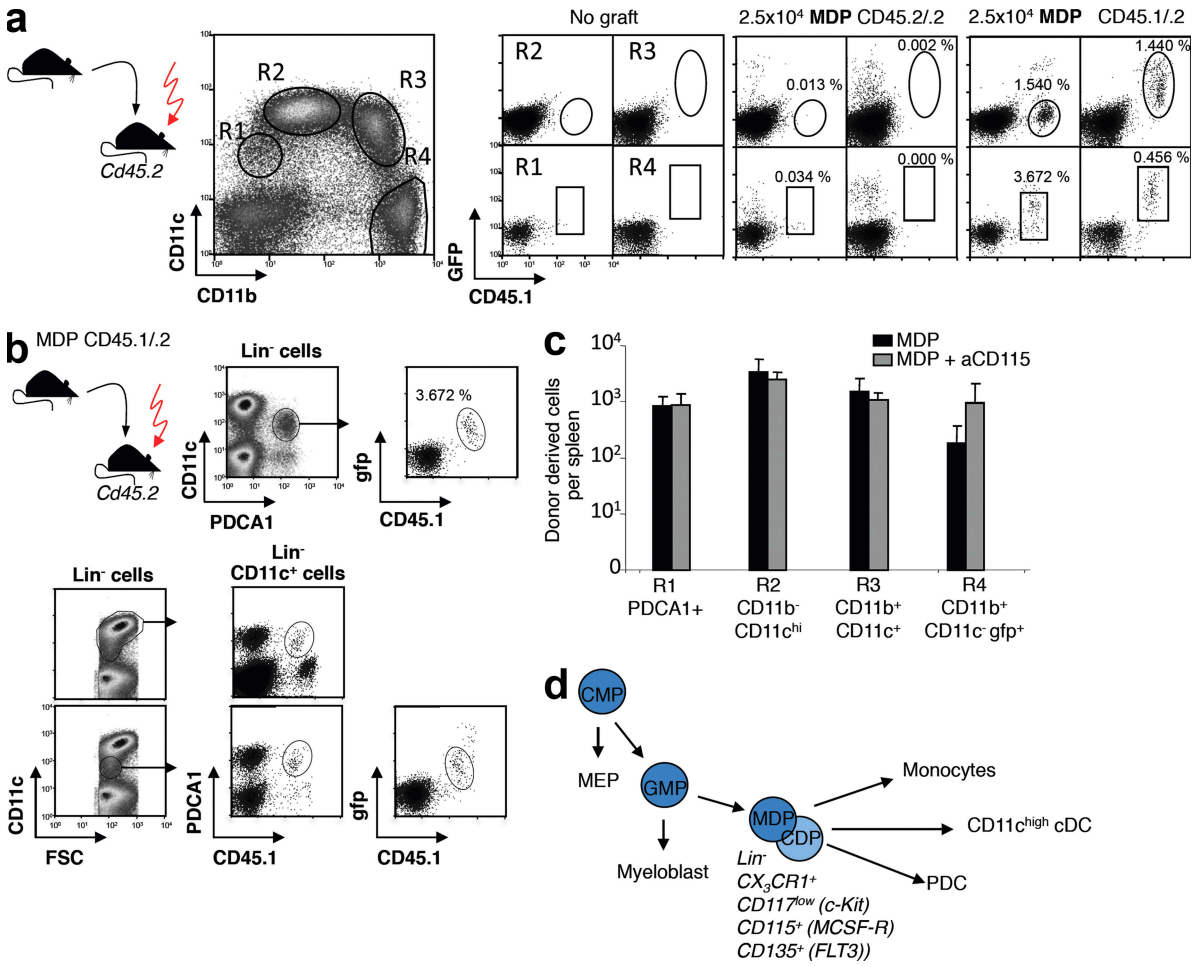

Figure 2. Differentiation potential of MDP in vivo. (a–c) MDPs from *Cd45.1/2* or *Cd45.2 Cx3cr1*$^{gfp/+}$ reporter mice were purified as described in Fig. S2 (available at http://www.jem.org/cgi/content/full/jem.20081385/DC1) and were adoptively transferred into irradiated (900 rad) C57BL/6 *Cd45.2* congenic recipients. Spleens of recipient mice were analyzed at day 7 after transfer by flow cytometry, using lineage marker (NK1.1 CD3 CD19), CD11b, CD11c, and CD8-α antibodies. R1 corresponds to PDCs (Lin$^-$ CD11c^{int} CD11b$^-$ CX_3CR1^+ cells), R2 and R3 correspond to cDCs (lin$^-$ CD11c^{high} CD11b$^-$ CX_3CR1^- cells and lin$^-$ CD11c^{high} CD11b$^+$ CX_3CR1^+ cells), and R4 corresponds to monocytes (lin$^-$ CD11b$^+$ CD11c$^-$ CX_3CR1^+ cells). The experiment was repeated five times with two to three mice per group and with similar results. (b) Donor-derived Lin$^-$ CD11c^{int} CD11b$^-$ CX_3CR1^+ cells express PDCA1. (c) Role of anti-CD115 Ab. The number of donor-derived cells per spleen are represented after adoptive transfer of MDP, purified with or without CD115 antibody (n = at least 3 mice per group from two experiments). Error bars show SD. (d) The flow diagram represent the Lin$^-$ CD117^{int} CD115$^+$ CD135$^+$ CX_3CR1^+ MDPs that give rise to monocytes, cDCs, and PDCs and their putative relationship with other myeloid precursors.

Published March 9, 2009

after infection and, thus, that accumulation of spleen monocytes during infection is not a result of their proliferation in the spleen. In addition, the proportion of splenic monocytes that bind annexin-V in *Lm*-infected mice was similar in CX_3CR1-deficient animals and in controls (Fig. S6), indicating that the apoptosis rate of CX_3CR1-deficient $Gr1^+$ monocytes during *Lm* infection was not increased in comparison with controls.

Early control of *Lm* growth in the spleen was also significantly less efficient in CX_3CR1-deficient mice on both BALB/c and C57BL/6 backgrounds (Fig. 4, h and i). Bacterial load in the spleen 24 h after an i.v. infection was 4× higher in BALB/c $Cx_3cr1^{-/-}$ mice in comparison with controls (Fig. 5 h) and at least twice as high in C57BL/6 (Fig. 4 i).

Altogether, these data indicate that CX_3CR1 is important for the recruitment of monocytes to the spleen in irradiated host and during *Lm* infection, and for the early control of bacteria growth. It is of note that the frequency of monocytes in the spleen of noninfected mice were not affected by CX_3CR1 deficiency (Fig. 4 d), indicating that CX_3CR1 is dispensable for the recruitment of monocytes in the spleen in the steady state but important during acute inflammation.

$CD115^+$ $Gr1^+$ monocytes recruited to the spleen during *Lm* infection differentiate into effector cells (TipDCs) that produce TNF, inductible nitric oxide synthase (iNOS), and reactive oxygen intermediates (ROIs)

Because the decreased recruitment of monocytes in the spleen during *Lm* infection in CX_3CR1-deficient mice correlated with a decreased bacterial clearance, we investigated whether monocytes recruited to the spleen may be involved in the control of *Lm* growth and express effector activities important for *Lm* clearance such as TNF-α secretion, iNOS expression, and reactive oxygen production. Monocytes have already been proposed to be precursors of TipDCs that accumulate to the spleen of mice infected with *Lm*, produce TNF-α and iNOS, and are needed for the control of primary infection (44–46). Recruited monocytes were the majority (90%) of the $CD115^+$ $Gr1^+$ subset (Fig. S7, available at http://www.jem.org/cgi/content/full/jem.20081385/DC1). In spleen, $lineage^-$ (Ly6G, NK1.1, CD3, and CD19) $CD11b^+$ $CD11c^-$ splenocytes were identified as monocytes based on their expression of CD115, Ly6C/Gr1, and F4/80 (Fig. 5 a) (32). We observed that these spleen $CD115^+$ $Gr1^+$ monocytes produced TNF-α, iNOS, and ROI in mice during infection

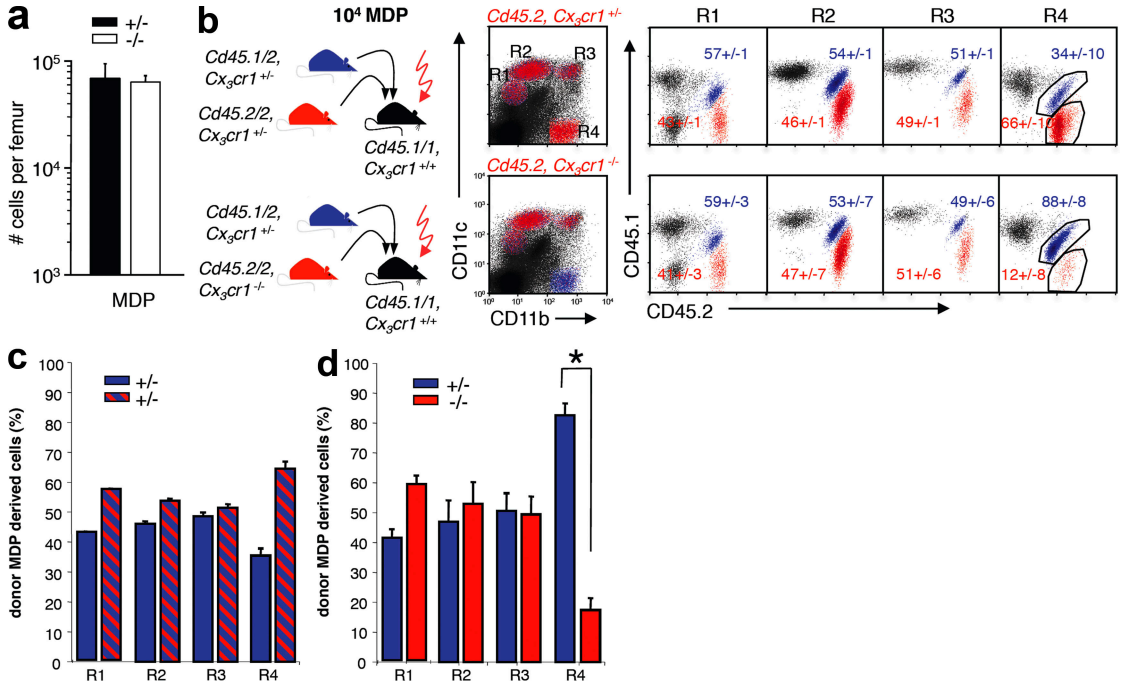

Figure 3. CX_3CR1 is important for the development of $CD11b^+$ $CD11c^-$ monocytes. (a) MDP numbers in BM from $CX_3CR1^{+/-}$ (black) and $CX_3CR1^{-/-}$ (white) mice. Data are the mean ± SD of five mice per group. (b–d) Competitive adoptive transfer of MDP into irradiated host (900 rad). Equal numbers (10^4) of MDPs from *Cd45.1/2* mice (blue) and *Cd45.2/2* mice (red) were mixed and adoptively transferred into a *Cd45.1* congenic recipient. Spleens of recipient mice were analyzed at day 7 after transfer by flow cytometry, using lineage marker (NK1.1 CD3 CD19), CD11b, CD11c, and CD8-α antibodies. (b and c) When both *Cd45.1/2* and *Cd45.2/2* donor mice were of the $Cx_3cr1^{+/-}$ genotype, both donors contributed equally to $NK1.1^-$ $CD3^-$ $CD19^-$ $CD11c^{high}$ $CD11b^-$ (R1, cDC) and $NK1.1^-$ $CD3^-$ $CD19^-$ $CD11c^{high}$ $CD11b^+$ (R2, cDC), $NK1.1^-$ $CD3^-$ $CD19^-$ $CD11c^{int}$ $CD11b^-$ (R3, PDC), and $NK1.1^-$ $CD3^-$ $CD19^-$ $CD11b^+$ $CD11c^-$ splenocytes (R4). (b and d) In contrast, when *Cd45.1/2* donor mice were of the $Cx_3cr1^{+/-}$ genotype and *Cd45.2/2* donor mice were of the $Cx_3cr1^{-/-}$ genotype (CX_3CR1 deficient), both donors contributed equally to $CD11c^+$ cDCs in R1 and R2 but CD45.1/2 $Cx_3cr1^{+/-}$ MDPs were 10× more efficient than CD45.2/2 CX_3CR1-deficient MDPs in generating $CD11b^+$ $CD11c^-$ splenocytes in R3. Results in b are from one representative experiment out of three, with two to three mice per experimental group, and bar graphs in c and d represent the mean and SD from three independent experiments. The asterisk indicates a significative difference between groups ($P < 0.05$ using the Wilcoxon test).

Published March 9, 2009

with *Lm* (Fig. 5, b–d; and Fig. S8) and were localized in the T cell area and in the perifollicular area of the spleen (Fig. 5 e). Altogether, these data therefore indicate that MDPs give rise to blood CD115$^+$ Gr1$^+$ monocytes, which are recruited to the spleen during infection via a process that involves CX_3CR1, and that these cells expressed effector functions that are important for *Lm* elimination.

Gr1$^+$ monocyte survival and MDP survival and proliferation are normal in CX_3CR1-deficient mice

Other mechanisms that might be responsible for the impaired accumulation of CX_3CR1-deficient CD115$^+$ Gr1$^+$ monocytes in the spleen include decreased survival or proliferation of monocytes or decreased survival, proliferation, or differentiation of MDP. As indicated by Fig. 4 g and Fig. S6, CX_3CR1-deficient Gr1$^+$ monocytes did not exhibit increased apoptosis rate during *Lm* infection, and the proliferation of monocytes in the spleen is not responsible for their accumulation. Total blood monocyte counts (CD115$^+$ CD11b$^+$ NK1.1$^-$) and Gr1$^+$ monocyte counts performed in *Cx$_3$cr1$^{+/+}$*, *Cx$_3$cr1$^{+/-}$*, *Cx$_3$cr1$^{-/-}$*, *Cx$_3$cl1$^{+/+}$*, and *Cx$_3$cl1$^{-/-}$* mice did not show any difference between CX_3CR1-deficient or CX_3CL1-deficient mice and control mice (Fig. S9, a–c), and the proportion of Gr1$^+$ blood monocytes that bind annexin-V in the steady state was also similar in CX_3CR1-deficient animals and in controls (Fig. S9 d). However, there was a 20% decrease in the numbers

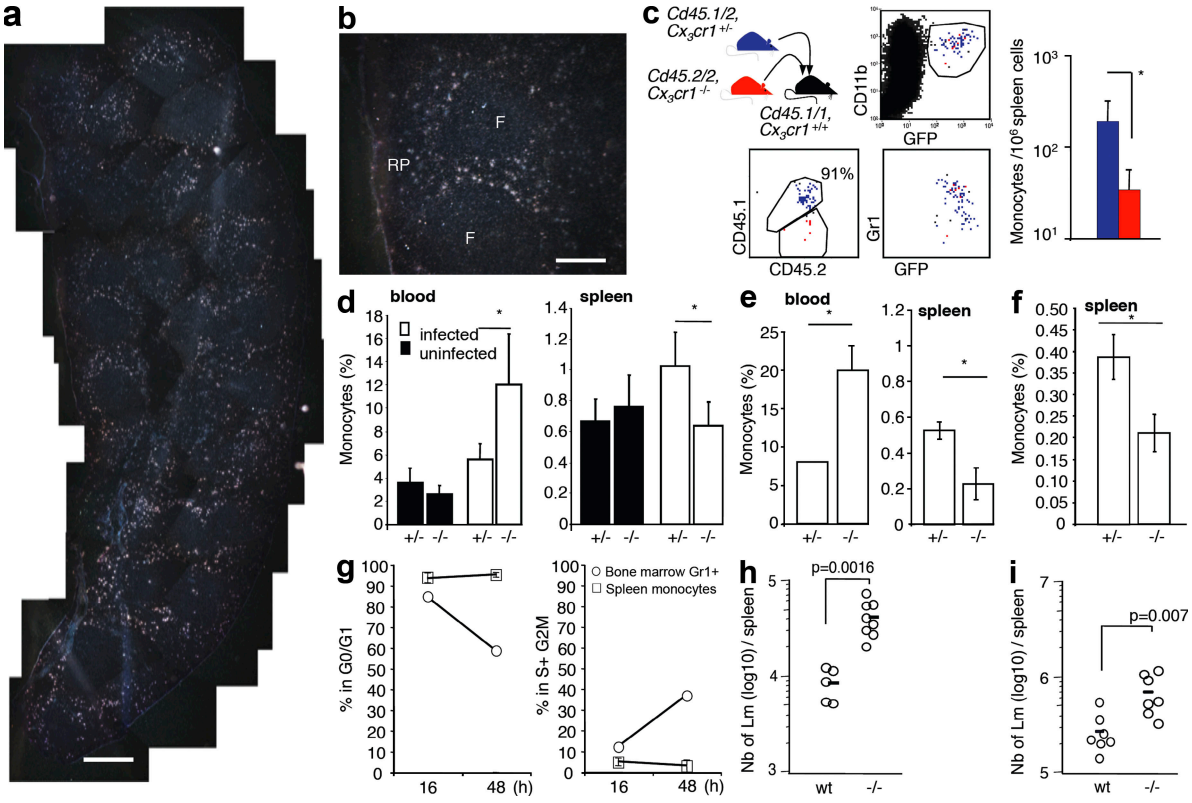

Figure 4. CX_3CR1 is important for the recruitment of CD11b$^+$ CD11c$^-$ monocytes to the spleen during infection. (a and b) Mouse fractalkine/CX_3CL1 transcripts are detected in spleen tissue sections from WT mice around B cells follicles in the marginal zone/T cell area. Bars: (a) 500 µm; (b) 200 µm. (c) Short-term adoptive transfer of BM monocytes into irradiated WT recipient mice. Equal numbers (2×10^5) of BM monocytes from *Cx$_3$cr1$^{+/-}$ Cd45.1/2* mice (blue) and *Cx$_3$cr1$^{-/-}$ Cd45.2/2* mice (red) were mixed and adoptively transferred into a *Cd45.1* congenic recipient. CX_3CR1-expressing CD45.1/2 Gr1$^+$ monocytes are recruited in the spleen of irradiated host 10× more efficiently than CX_3CR1-deficient monocytes. The experiment was performed three times with two to three mice per group with similar results. (d–f) Monocyte recruitment in the spleen of infected mice. (d) BALB/c Cx$_3$cr1$^{+/-}$ and Cx$_3$cr1$^{-/-}$ mice (seven per group) were infected i.v. with live *Lm* (3×10^5), and monocytes (CX_3CR1^- gfp$^+$ CD11b$^+$ Ly-6C$^+$ Ly-6G$^-$, CD19$^-$, CD3$^-$, and NK1.1$^-$) were enumerated after 24 h in the blood and spleen of infected and control uninfected mice. (e) C57BL/6 Cx$_3$cr1$^{+/-}$ and Cx$_3$cr1$^{-/-}$ mice (seven per group) were injected with 7×10^5 *Lm*, and monocytes were enumerated after 24 h in the blood and spleen of infected mice. (f) C57BL/6 Cx$_3$cr1$^{+/-}$ and Cx$_3$cr1$^{-/-}$ mice (seven per group) were injected with 7×10^3 *Lm*, and monocytes were enumerated after 48 h in the spleen of infected mice. *Lm* growth in the spleen of infected mice is shown. The asterisks indicate a significative difference between groups ($P < 0.05$). (g) Absence of proliferation of monocytes in the spleen of *Lm*-infected mice. BALB/c mice ($n = 6$ per group) were infected with 3×10^3 bacteria, spleen and leg bones were harvested 16 and 48 h later, and cells were processed as indicated in Fig. S5 (available at http://www.jem.org/cgi/content/full/jem.20081385/DC1). Data indicate the percentage of BM precursors and spleen monocytes in G0/G1 and in G2$^+$S as analyzed by flow cytometry after DNA labeling with PI. The experiment was performed three times with similar results. (h) BALB/c Cx$_3$cr1$^{+/+}$ and Cx$_3$cr1$^{-/-}$ mice were infected i.v. with live *Lm* (3×10^3). Data show the number of bacteria (mean ± SE) in the spleen 24 h after infection. (i) C57BL/6 Cx$_3$cr1$^{+/+}$ and Cx$_3$cr1$^{-/-}$ mice were injected with 10^4 *Lm*. Data show the number of bacteria (mean ± SE) in the spleen 24 h after infection. Circles represent individual mice.

Published March 9, 2009

of blood Gr1$^-$ monocytes in CX_3CR1-deficient and CX_3CL1-deficient mice in comparison with controls (Fig. S9, a–c), and the frequency of apoptotic Gr1$^-$ monocytes was higher in *Cx$_3$cl1$^{-/-}$* mice in comparison with WT mice (Fig. S9 d).

The clonogenic and proliferation potentials of MDPs were then studied in vitro in the presence or absence of CX_3CL1/fractalkine. CX_3CR1/CX_3CL1 did not confer any advantage in terms of growth or survival, even in competition with WT cells (Fig. S10, a–c, available at http://www.jem.org/cgi/content/full/jem.20081385/DC1). The role of CX_3CR1 in the proliferation of MDP-derived cells in vivo was investigated by labeling MDP and CD19$^+$ B cells, as a control, with Cell Tracker 633 (BODIPY 630/650 MeBr) and carrying out the adoptive transfer of these cells into irradiated recipients. 6 d later, 100% of both *Cx$_3$cr1$^{+/-}$* and *Cx$_3$cr1$^{-/-}$* MDP-derived cDCs and monocytes were no longer labeled (Fig. S10 d), indicating they that had undergone multiple rounds of division. Together with results from the adoptive transfer experiments depicted in Fig. 4, these data indicate that CX_3CR1 deficiency does not significantly affect the proliferation and differentiation potential of MDP.

DISCUSSION

This study investigated the differentiation potential of the CX_3CR1^+ MDPs and the role of CX_3CR1 in their development. First, our data confirmed that CX_3CR1 was associated with the commitment of myeloid progenitors to the monocyte/macrophage/DC lineage. The recently described CDP (24, 25) also expresses CX_3CR1, CD115, and FLT3, and its phenotype was overlapping with the MDP (this study and

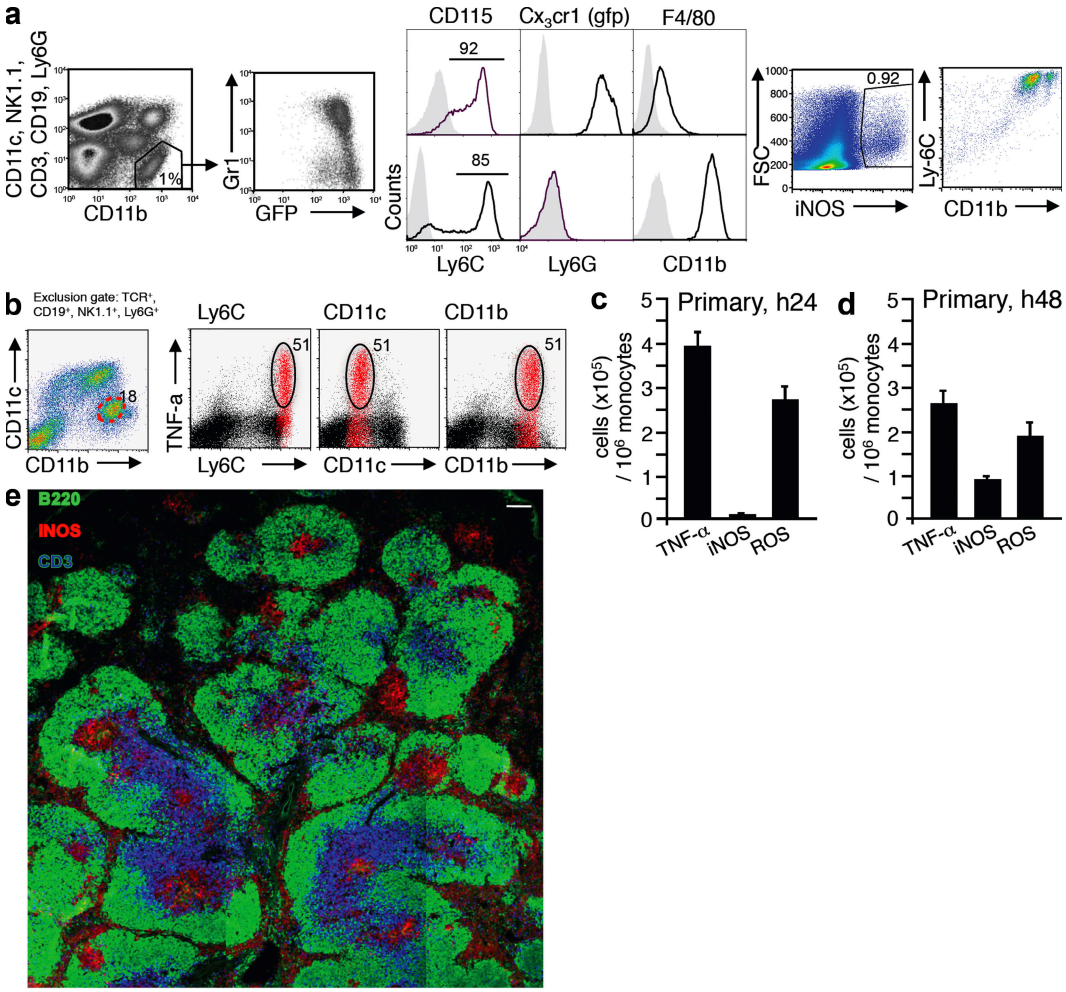

Figure 5. Functions of spleen CD115$^+$ Gr1$^+$/TipDCs. (a) CD11b$^+$ spleen cells from $Cx_3cr1^{gfp/+}$ reporter mice negative for lineage marker (NK1.1, CD3, B220, CD19, and CD11c) were analyzed for Ly6G, Ly6C, F4/80, CD115, and CX_3CR1 (gfp) expression by multicolor flow cytometry. (b) TNF production by lineage$^-$ CD11c^{low} CD11b$^+$ cells 24 h after i.v. infection with *Lm*. Gated cells (circled) are displayed in red. Data show representative FACS profiles from three experiments. (c and d) Production of TNF-α, iNOS, and ROI by lineage$^-$ CD11c^{low} CD11b$^+$ Gr1$^+$/Ly6C$^+$ spleen cells from C57BL/6 mice 24 (c) and 48 h (d) after i.v. infection with 7×10^5 bacteria and 7×10^3 bacteria, respectively. The experiment was repeated five times with similar results. Error bars show SD. (e) iNOS$^+$ cells in the spleen of BALB/c mice 24 h after infection with 10^5 WT *Lm* (red) express CD11b and Ly6C and are found in the perifollicular area and T cell area. B cell follicles are labeled with anti-B220 antibodies (green) and T cells are labeled with anti-CD3 antibodies (blue). Bar, 100 µm. The experiment was repeated five times with similar results.

Published March 9, 2009

reference 9). MDP can give rise to both DCs (PDCs and cDCs) and monocytes/macrophages but do not have the potential to give rise to granulocytes. Thus, they have a more restricted differentiation potential than CMPs, which can give rise to all myeloid cells, and GMPs, which can give rise to granulocytes, macrophages, and DCs (Fig. 2 d). CDP has been reported to give rise to cDCs and PDCs but not macrophages and, thus, has a more restricted differentiation potential than MDPs and may be placed downstream (Fig. 2 d). Further studies will be needed to investigate the developmental relationship between MDPs and CDPs.

CX_3CR1 is a later marker than CSF-1R in myeloid lineage commitment. In this study, we investigated the role of CX_3CR1/CX_3CL1 in the development of MDP-derived cells by studying mice lacking CX_3CR1 or its ligand CX_3CL1/fractalkine during acute and chronic inflammation and in a sensitive competitive adoptive transfer model. This study revealed an important role of CX_3CR1 in the recruitment of $CD115^+$ $Gr1^+$ inflammatory monocytes, which are immediate precursors to TipDCs, to the spleen during infection and for the control of bacterial growth during primary infection in two different strains of mice (C57BL/6 and BALB/c).

Impaired recruitment of CX_3CR1-deficient $Gr1^+$ monocytes/TipDCs is the most likely mechanism underlying our observations for the following reasons: in situ hybridization experiments (Fig. 4 and Fig. S4) indicated that fractalkine is expressed in the marginal zone/T cell areas of the spleen, where TipDC accumulate during infection (Fig. 5) (44); short-term adoptive transfer of BM monocytes into irradiated hosts decreased the accumulation of CX_3CR1-deficient monocytes in the spleen by a factor of ten (see Fig. 4); during acute *Lm* infection, the number of monocytes was higher in the blood of infected CX_3CR1-deficient mice but decreased in the spleen (Fig. 4), and the frequency of annexin-V^{high} monocytes was not increased in spleen from infected CX_3CR1-deficient mice (Fig. S6); CX_3CR1 deficiency does not appear to influence the survival of $CD115^+$ $Gr1^+$ monocytes in the periphery (Fig. S9); and finally, we have found that CX_3CR1 was redundant for MDP development, survival, homing to the spleen, and differentiation in vivo and in vitro (Fig. S10) and MDP-derived spleen cDCs and PDCs appear to develop normally.

It is of note that although $CD115^+$ $Gr1^+$ (CX_3CR1^{low}) inflammatory monocytes were present in normal numbers in both CX_3CR1- and CX_3CL1-deficient mice, the present data confirm that CX_3CR1 deficiency also slightly decreases the survival of the $CD115^+$ $Gr1^-$ monocytes (Fig. S9). This result was expected and consistent with the conclusions that we made from our earlier adoptive transfer experiments (29) and with a more recent study (47). CX_3CR1 has been previously shown to be important for the adhesion of $CD115^+$ $Gr1^-$ (CX_3CR1^{high}) monocytes to the endothelium of blood vessels (38, 42). The mechanism underlying the selective survival defect of $CD115^+$ $Gr1^-$ CX_3CR1^{high} monocytes may thus be related to the unique patrolling behavior of these cells, which attach themselves to the luminal side of the endothelium via a CX_3CR1- and LFA1-dependent mechanism, crawling onto the endothelium for considerable periods of time without extravasation (42). Human CX_3CR1^{high} cells also adhere to the endothelium via a CX_3CR1-dependent mechanism (38), and adhesion is known to increase survival as has been shown for CX_3CR1-expressing cells binding to CX_3CL1 via a mechanism involving an Akt/GSK-3β–mediated antiapoptotic signaling pathway (48, 49).

The role of CX_3CR1 for the recruitment of $CD115^+$ $Gr1^+$ monocytes/TipDC precursors is reminiscent of the phenotype of CCR2-, MCP1-, and MCP3- deficient mice (45, 50). However, the disruption of the CCR2 axis results in a much more dramatic phenotype because both $Gr1^+$ monocytes exit from the BM into the bloodstream, and the recruitment into tissues of the few monocytes that exit the BM is impaired in these mice (45, 46, 50). Thus CCR2-deficient mice have reduced numbers of TipDCs. In contrast, BM output is intact in CX_3CR1-deficient mice, the number of blood $Gr1^+$ monocytes are normal, and only their recruitment is impaired. Similarly, CCR2-deficient mice have a dramatically impaired innate response to *Lm* infection and die of infection within a few days (46), whereas CX_3CR1-deficient hosts exhibit a reduced clearance of *Lm* at 24 h after infections (Fig. 3), but at later time points we did not observe significant differences in the survival of CX_3CR1-deficient and control mice (not depicted). We therefore propose that CX_3CR1 may play an important role in mediating the recruitment of $CD115^+$ $Gr1^+$ inflammatory monocytes in the white pulp of the spleen during acute inflammation, possibly through adhesion to the capillary endothelial cells of the marginal zone of the spleen.

MATERIALS AND METHODS

Animals. C57BL/6 mice on *Cd45.2* or *Cd45.1* congenic backgrounds were obtained from Charles River Laboratories. Cx_3cr1^{gfp} reporter mice on the C57BL/6 and BALB/c background were obtained from D. Littman's laboratory (Skirball Institute, New York, NY). $Cx_3cr1^{gfp/gfp}$ C57BL/6 mice were crossed with WT *Cd45.1* mice to produce $Cx_3cr1^{gfp/+}$ mice on a mixed *Cd45.1/Cd45.2* background for competitive adoptive transfer experiments. C57BL/6 $Cx_3cr1^{+/+}$, $Cx_3cr1^{gfp/+}$, and $Cx_3cr1^{gfp/gfp}$ and BALB/c $Cx_3cr1^{+/+}$ and $Cx_3cr1^{gfp/gfp}$ were bred and maintained in the specific pathogen-free animal facility of the Institut Fédératif de Recherche (IRF) Necker-Enfants Malades and of the Institut National de la Santé et de la Recherche Médicale U924. C57BL/6 $Cx_3cl1^{+/+}$ and $Cx_3cl1^{-/-}$ and $ApoE^{-/-}$ $Cx_3cl1^{+/+}$ and $Cx_3cl1^{-/-}$ mice were maintained in the laboratory of I.F. Charo (Gladstone Institute of Cardiovascular Disease, University of California, San Francisco, San Francisco, CA). All mice were maintained according to institutional guidelines and used at the age of 8–14 wk old. 4-wk-old C57BL/6 mice on the *Cd45.1* background were used as adoptive transfer recipients. Experimental protocols using mice were examined and approved by the Direction Departementale des Services Vétérinaires de Paris (Paris, France).

Antibodies and recombinant proteins. The following purified or conjugated antibodies were purchased from BD: purified anti-FcγRIII/II (CD32/16, clone 2.4G2); PE-, APC-, PcP-, or biotin-labeled anti-CD11b (M1/70); PE-, APC-, or biotin-labeled anti-CD117 (cKit; 2B8); PE- or APC-labeled anti-NK1.1 (PK136); FITC-, PE-, or APC-labeled anti-CD11c (HL3); PE- or APC-labeled anti–TCR-β (H57-597); PE- or APC-labeled anti-B220 (RA3-6B2); biotin-labeled anti-CD45.2 (104); FITC- or biotin-labeled anti-Ly6C (AL-21); PE-labeled anti-Ly6G (1A8); PE-Cy7–labeled anti–CD8-α (53–6.7); PerCP-labeled anti-CD4 (RM4-5); PE-labeled anti-CD3 (145-2C11); PE-labeled anti-CD19 (MB19-1); APC-labeled anti–TNF-α (MP6-XT22); and control rat IgG_1 mAb. The following antibodies were purchased from eBioscience: PE-Cy7–labeled anti-CD45.1 (A20),

Published March 9, 2009

APC–Alexa Fluor 750-labeled anti-CD45.2 (104), PE- or PE-Cy5–labeled anti-Flt3 (A2F10), and PE- or biotin-labeled anti CD115 (AFS98). Anti-CD169 (MOMA-1) and APC- or biotin-labeled F4/80 clone Cl:A3-1 were purchased from AbD Serotec. mPDCA1 antibody was purchased from Miltenyi Biotec. Anti–NOS-2 (M-19) polyclonal rabbit was purchased from Santa Cruz Biotechnology, Inc. Goat anti–rabbit Alexa Fluor 647 was purchased from Invitrogen. Hydroethidine was purchased from Polysciences, Inc. Antibodies used for depletion, including TER-119 (erythrocytes), RB6-8C5 (Ly6-C/G), and GK1.5 (CD4), were supernatants of hybridomas donated by B. Rocha (IFR Necker, Paris, France). Streptavidin Pacific Blue was purchased from Invitrogen. Dead cells were gated out by PI labeling (Invitrogen). APC-labeled annexin V was purchased from BD. Recombinant mouse macrophage CSF-1 and recombinant mouse fractalkine (CX_3CL1) were purchased from R&D Systems. Recombinant mouse GM-CSF was purchased from PeproTech.

Mouse blood phenotyping. Blood was drawn according to institutional guidelines, and red blood cells were lysed in 5 vol of red blood cell lysis buffer (155 mM NH_4Cl, 10 mM $NaHCO_3$, and 0.1 mM EDTA). Cell suspensions were filtered using a 40-µm filter (BD), washed twice in PBS 0.5% BSA, and an aliquot was counted with a Guava ViaCount analyzer (Guava Technologies). Cells were incubated with anti–mouse FcRII/III (2.4G2) for 10 min at 4°C in PBS 0.5% BSA and then stained with anti–mouse antibodies specific for CD11b (PE-Cy7), Ly6C (biotin), NK1.1 (APC), and CD115 (PE). Biotinylated antibodies were revealed by subsequent staining with streptavidin–Pacific blue. Cells were analyzed on a nine-color CYAN ADP flow cytometer (Dako) using the Summit 4.3 software (Dako), and monocytes were identified as $CD115^+$, $CD11b^+$, SSC^{lo}, $NK1.1^-$, or $Ly6c^{+or-}$ cells. Annexin V staining was performed according to the manufacturer's instructions. Absolute numbers were calculated using cell percentages and total white blood cells counts. Data on blood monocytes counts were obtained from littermate mice at the age of 7–8 wk for $Cx_3cr1^{+/+}$, $Cx_3cr1^{gfp/+}$, and $Cx_3cr1^{gfp/gfp}$ mice and 13–14 wk old mice for $Cx_3cl1^{+/+}$ and $Cx_3cl1^{-/-}$ mice.

Phenotyping of splenocytes. Spleens were removed, triturated in RPMI 2% FCS at 4°C with the end of a 3-ml syringe, and then passed through a 100-µm cell strainer (BD) in one well of a 6-well plate. Cell suspensions were filtered using a 40-µm filter, washed twice in PBS 0.5% BSA, blocked with anti–mouse FcRII/III, and then stained with anti–mouse antibodies specific for CD3e, CD11c, CD19, Ly6G, CD11b, Ly6C, mPDCA1, NK1.1, and CD115. Biotinylated antibodies were revealed by subsequent staining with streptavidin–Pacific blue. Annexin V staining was performed according to the manufacturer's instructions. Cells were analyzed on a CYAN ADP flow cytometer using Summit 4.3 software (Dako).

Phenotyping, isolation, and adoptive transfer of MDP and CDP. BM cells from femurs and tibias of $Cx_3cr1^{gfp/+}$ mice aged 6 wk were flushed with serum-free RPMI, Fc receptors were blocked with antibody to FcγRIII/II (2.4G2), and cells were labeled using antibodies against lineage markers (IL7-Rα, CD11c, CD11b, NK1.1, CD3, Ter119, CD19, and Gr1), CD117, CD115, and CD135. For purification of MDP, red blood cells and Gr1-expressing cells were removed using Ter119 and RB68C5 antibodies as previously described (22). MDP (defined as IL7-$R\alpha^-$ $lineage^-$ gfp^+ [CX_3CR1] $CD117^{int}$ expressing CD115; Fig. S2), CDP (defined as IL7$R\alpha^-$ $lineage^-$ $CD135^+$ $CD115^+$ $CD117^{int}$; Fig. S3), and BM monocytes (defined as gfp^+ $CD11b^+$ $CD115^+$ $NK1.1^-$ $CD117^-$) were purified by flow cytometry using FACSVantage or FACSAria cell sorters (BD). For competitive adoptive transfers, monocytes or MDP were purified from $Cx_3cr1^{gfp/gfp}$ mice on a *Cd45.2* background and from $Cx_3cr1^{gfp/+}$ mice on a *Cd45.2/.1* background, unless otherwise indicated. FACS-purified cells from each genetic background were mixed at a 1:1 ratio and were transferred i.v. to 4-wk-old recipient mice on a *Cd45.1* background. Recipients were either irradiated with 10 Gy or were not irradiated. For analysis of cell populations in WT mice, Cx_3cr1^{gfp} reporter mice, and adoptive transfer recipients, blood and organs were harvested from anaesthetized mice as described previously (29), and spleens were digested with collagenase D, homogenized, and filtered. Erythrocytes were lysed using red blood cell lysis buffer for quantification of cell populations in reporter mice or were depleted by density gradient centrifugation (LSM 1077; Eurobio) for analysis of adoptive transfer recipients. PBMC or splenic mononuclear cell suspensions were enumerated with a Guava Viacount analyser. Fc receptors were blocked, and then cells were labeled using fluorochrome- or biotin- conjugated antibodies and analyzed by five, six, or seven-color flow cytometry using a Cyan ADP.

For in vivo proliferation assays, splenocytes or FACS-sorted MDP were labeled using BODIPY far-red cell tracker (Invitrogen), transferred to congenic recipients, and analyzed by flow cytometry after 5 d. Cell division of MDP-derived cells was assessed by comparison with nondividing $B220^+$ B lymphocytes.

In vitro analysis of cell survival, proliferation, and differentiation potential. MDPs from $Cx_3cr1^{+/-}$ or $Cx_3cr1^{-/-}$ were purified by FACS, as described in the previous section, and plated at one cell per well into 96-well plates containing Opti-MEM (Invitrogen) supplemented with 10% FCS (PAN biotech), 100 U/ml penicillin, and 100 µg/ml streptomycin (Invitrogen) along with CSF-1, GM-CSF, or both (10 ng/ml each unless otherwise indicated) in the presence or absence of recombinant CX_3CL1. Resulting colonies were enumerated after incubation at 37°C in 5% CO_2 for 7 d. For differentiation analysis, colonies were recovered from wells by vigorous pipetting and were immunolabeled for cell surface markers as described in the previous section. For determination of proliferation potential, individual cells from colonies arising from single cell clones were counted using a 10 or 5× objective on a microscope (Axiovert; Carl Zeiss, Inc.). Counting accuracy was validated by digital analysis of random colonies of various sizes photographed using a camera (CoolSnap ES; Roper Scientific) and Photoshop CS (Adobe) for marking of individual cell bodies.

For analysis of proliferation under competitive conditions, 100 MDPs each from $Cx_3cr1^{+/-}$ and $Cx_3cr1^{-/-}$ mice on different CD45 congenic backgrounds, as described in the Animals section, were deposited into wells of 96-well round-bottom plates, coated with fractalkine or BSA as control, and grown in decreasing concentrations of CSF-1. After 5 d in culture, cells were harvested from individual wells and analyzed for origin by CD45.1 and CD45.2 staining by flow cytometry. At least 10 wells were analyzed per experiment.

***Lm* infection.** The *Lm* 10403s WT strain was used in these experiments. This strain exhibit an LD_{50} of 7×10^4 in C57BL/6 mice. Bacteria were prepared from clones grown from organs of infected mice. Stocks of bacteria were kept frozen at −80°C. For infections, bacteria were grown to a logarithmic phase (OD_{600} = 0.05–0.15) in Broth Heart Infusion medium (Sigma-Aldrich), diluted in PBS, and injected i.v. into lateral tail vein with 0.1–10× LD_{50} of WT *Lm* per mouse. To study production of TNF and iNOS, organs were cut in small pieces and incubated at 37°C for 20 min in HBSS medium (Invitrogen) containing 4,000 U/ml collagenase I (Invitrogen) and 0.1 mg/ml DNase I (Roche). Red blood cells were lysed for 2–3 min in 170 mM NH_4Cl and 17 mM Tris HCl, pH 7.4. Cells were stained with the specified antibodies in 100 ml PBS containing 0.5% of BSA (FACS buffer). For the TNF-α intracellular staining, splenocytes were incubated at 37°C and 5% CO_2 for 3–4 h in RPMI 1640 (Invitrogen) containing 5% FCS and 2 mg/ml Golgi Plug (BD) with or without 5×10^8 HKLM/ml. Cells were incubated for 20 min on ice with the indicated cell surface marker mAbs, fixed in 1% PFA FACS buffer for 20 min on ice, and permeabilized for 30 min in Perm/Wash (BD). For intracellular staining of TNF-α, cells were incubated for 20 min on ice in FACS buffer containing anti–TNF-α or control rat IgG_1. For intracellular staining of iNOS, cells were incubated for 20 min on ice in FACS buffer containing anti-iNOS rabbit polyclonal or control normal goat IgG, and staining was revealed using goat anti–rabbit Alexa Fluor 647 mAb. In all cases, cells were washed, fixed for 30 min in 1% PFA FACS buffer, and analyzed on a FACSCalibur cytofluorometer (BD). To study the production of ROI, $5–10 \times 10^6$ splenocytes were incubated for 3 h at 37°C and 5% CO2 in 5% FCS RPMI 1640 with 5×10^8 HKLM/ml and 160 µM hydroethidine. Hydroethidine is oxidized by ROI in red fluorescent ethidium bromure, therefore allowing for the detection

Published March 9, 2009

of ROI-producing cells. Cells were washed in FACS buffer and stained for expression of cell surface markers. To measure bacterial titers in the spleen, mice were injected i.v. into the lateral tail vein with 10^4 WT *Lm* and organs were harvested and dissociated on metal screens in 10 ml of 0.1% Triton X-100 (Sigma-Aldrich). Serial dilutions were performed in the same buffer, and 50 µl was plated onto BHI media plates.

For cell cycle analysis, 6-wk-old BALB/c mice were infected with 3×10^3 bacteria. 48 h later, spleen and leg bones were harvested. BM were flushed with RPMI 5% FCS and spleen were treated with collagenase/DNase. After lysis of red blood cells, cells suspensions were separately enriched for CD11b (MACs) and stained for CD11b, Ly6c, DX5, CD3, CD19, and Ly6G surface markers. Monocytes ($CD11b^+$ $Ly6C^+$ $DX5^-$ $CD3^-$ $CD19^-$ $Ly6G^-$) were sorted, and splenic monocytes from individual mice were treated independently for cell cycle, whereas monocytes from BM were pooled. Cell cycle is defined as the following: cells were washed in PBS and fixed in 70% EtOH at 4°C for 30 min. Samples were then stained with 50 µg/ml PI in PBS complemented with 50 µg/ml RNase at 37°C for 30 min. Samples were then analyzed by flow cytometry.

Immunofluorescence. Spleens were fixed for 1 h in medium containing 0.05 M phosphate buffer, 0.1 M L-lysine, pH 7.4, 2 mg/ml $NaIO_4$, and 40 mg/ml paraformaldehyde and then dehydrated overnight at 4°C in a solution of 30% sucrose under agitation. Tissues were snap frozen in Tissue-Tek (Sakura). 10-µm frozen sections were stained with Alexa Fluor 488 anti-B220 antibody (RA36B2; BD), Alexa Fluor 647 anti-CD3 antibody (17A2; BD), and unconjugated anti-NOS2 antibody (M19; Santa Cruz Biotechnology, Inc.). NOS2 staining was revealed with an Alexa Fluor 647 goat anti–rabbit IgG (Invitrogen). Immunofluorescent confocal microscopy was performed with a laser-scanning confocal microscope (TCS SP5; Leica). Final image processing was performed using ImageJ software (National Institutes of Health).

RT PCR. Standard methods were used for the preparation of total cellular RNA and first-strand complementary DNA from spleens and brains of WT C57BL/6 mice. The following primer pairs were used: *Cx_3cl1* forward, 5′-CATGTGCGACAAGATGACCTCA-3′, and reverse, 5′-TTCCAATGCTCTGAGGCTTAGC-3′ (455-bp product); and *cyclophilin* forward, 5′-TGGTCAACCCCACCGTGTTCTTCG-3′, and reverse, 5′-TCCAGCATTTGCCATGGACAAGA-3′ (455-bp product).

In situ hybridization. The 60-mer oligonucleotide probes were synthesized and purified by Invitrogen. The oligonucleotides were 3′ end labeled with [^{35}S]dATP (PerkinElmer) using 15 U/ml of terminal deoxyribonucleotidyl transferase (Invitrogen) to a specific activity of $\sim 7 \times 10^8$ cpm/mg. The probes were purified on BioSpin columns (Bio-Rad Laboratories) before use. The Cx_3cl1 probes were chosen according to the human Cx_3cl1 complementary DNA sequence (available under GenBank accession no. NM_009142; http://www.ncbi.nlm.nih.gov/Genbank). The sequences of the probes were 5′-CCGGAGGCCACCCTAGACCACTATTCACTTATCAGAGACAGAGCAGGTGACCTTCCAGCT-3′ for the Cx_3cl1 sense probe (position 1443–1503) and 5′-AGCTGGAAGGTCACCTGCTCTGTCTCTGATAAGTGAATAGTGGTCTAGGGTGGCCTCCGG-3′ for the Cx_3cl1 antisense probe (position 1503–1443).

The hybridization cocktail contained 50% formamide, 4× SSC, Denhardt's solution, 0.25 mg/ml of yeast transfer RNA, 0.25 mg/ml of sheared herring sperm DNA, 0.25 mg/ml poly A^+, 10% dextran sulfate (Sigma-Aldrich), 100 mmol DTT, and [^{35}S]dATP-labeled probes (10^6 cpm/100 µl final concentration). 100 µl of hybridization solution was applied to each section. Sections were covered with a parafilm coverslip and incubated in a humidified chamber at 43°C for 20 h. After hybridization, the slides were washed twice for 15 min in SSC supplemented with 10 mM DTT at 55°C, twice for 15 min in 0.5× SSC supplemented with 10 mM DTT at 55°C, and, finally, in 0.5× SSC supplemented with 10 mM DTT for 15 min at room temperature. The sections were dipped in water, dehydrated by incubation in a series of graded concentrations of ethanol, placed against x-ray film (Hyperfilm Betamax; GE Healthcare) for 10 d, and then against photographic emulsion (NTB2; Eastman Kodak) for 2 mo at 4°C. Sections were developed, counterstained with toluidine blue (0.2% in 0.2 M sodium acetate, pH 4.3), covered with a coverslip, and examined under bright- or dark-field illumination with a light microscope (DNRB2; Leica). Both bright- and dark-field images were collected by a charge-coupled device camera (Nikon) connected to a computer.

Online supplemental material. Fig. S1 shows the expression of CX_3CR1 by PDCs. Fig. S2 shows the sorting gates for MDPs. Fig. S3 shows the effects of the AFS98 anti-CD115 antibody on the response of MDP to M-CSF in vitro. Fig. S4 shows the expression of CX_3CL1 in the spleen. Fig. S5 shows analysis of the proliferation of monocytes in the spleen and BM. Figs. S6 and S7 show the ratio of $Gr1^+$ and $Gr1^-$ monocytes in the spleens of infected and control mice and the frequency of annexin-V–positive cells. Fig. S8 describes the analysis of the production of TNF, NOS2, and ROI by $Gr1^+$ monocytes in the spleen of infected and controls mice. Fig. S9 indicates the absolute numbers of $Gr1^+$ and $Gr1^-$ monocytes in the blood of mice deficient in CX_3CR1 or CX_3CL1 in comparison to controls. Fig. S10 describes the role of CXRCR1 in the proliferation of MDP in vitro and in vivo. Online supplemental material is available at http://www.jem.org/cgi/content/full/jem.20081385/DC1.

C. Auffray, D.K. Fogg, and B. Senechal were supported by Institut National de la Santé et de la Recherche Médicale. E. Narni-Mancinelli and L. Campisi are both recipients of a Ministéro de l'Education Nationale de la Recherche et de la Technologie fellowship from the French ministry of research. This work was supported by an European Young Investigator (EURYI) award to F. Geissmann, grants from Institut National de la Santé et de la Recherche Médicale (Avenir) and Human Frontier Science Program (CDA) to G. Lauvau, grants from the Agence Nationale de la Recherche (ANR IRAP2005) to F. Geissmann and G. Lauvau, and grants from the Fondation pour la Recherche Medicale to F. Geissmann (Equipe FRM 2006) and to G. Lauvau (FRM equipments fund).

The authors have no conflicting financial interests.

Submitted: 27 June 2008
Accepted: 9 February 2009

REFERENCES

1. Sasmono, R.T., D. Oceandy, J.W. Pollard, W. Tong, P. Pavli, B.J. Wainwright, M.C. Ostrowski, S.R. Himes, and D.A. Hume. 2003. A macrophage colony-stimulating factor receptor-green fluorescent protein transgene is expressed throughout the mononuclear phagocyte system of the mouse. *Blood*. 101:1155–1163.
2. MacDonald, K.P., V. Rowe, H.M. Bofinger, R. Thomas, T. Sasmono, D.A. Hume, and G.R. Hill. 2005. The colony-stimulating factor 1 receptor is expressed on dendritic cells during differentiation and regulates their expansion. *J. Immunol*. 175:1399–1405.
3. Banchereau, J., and R.M. Steinman. 1998. Dendritic cells and the control of immunity. *Nature*. 392:245–252.
4. Gordon, S. 2002. Pattern recognition receptors: doubling up for the innate immune response. *Cell*. 111:927–930.
5. Taylor, P.R., and S. Gordon. 2003. Monocyte heterogeneity and innate immunity. *Immunity*. 19:2–4.
6. Shortman, K., and Y.J. Liu. 2002. Mouse and human dendritic cell subtypes. *Nat. Rev. Immunol*. 2:151–161.
7. Lin, H., E. Lee, K. Hestir, C. Leo, M. Huang, E. Bosch, R. Halenbeck, G. Wu, A. Zhou, D. Behrens, et al. 2008. Discovery of a cytokine and its receptor by functional screening of the extracellular proteome. *Science*. 320:807–811.
8. Dai, X.M., G.R. Ryan, A.J. Hapel, M.G. Dominguez, R.G. Russell, S. Kapp, V. Sylvestre, and E.R. Stanley. 2002. Targeted disruption of the mouse colony-stimulating factor 1 receptor gene results in osteopetrosis, mononuclear phagocyte deficiency, increased primitive progenitor cell frequencies, and reproductive defects. *Blood*. 99:111–120.
9. Waskow, C., K. Liu, G. Darrasse-Jeze, P. Guermonprez, F. Ginhoux, M. Merad, T. Shengelia, K. Yao, and M. Nussenzweig. 2008. The receptor tyrosine kinase Flt3 is required for dendritic cell development in peripheral lymphoid tissues. *Nat. Immunol*. 9:676–683.

10. Kabashima, K., T.A. Banks, K.M. Ansel, T.T. Lu, C.F. Ware, and J.G. Cyster. 2005. Intrinsic lymphotoxin-beta receptor requirement for homeostasis of lymphoid tissue dendritic cells. *Immunity*. 22:439–450.
11. Maraskovsky, E., K. Brasel, M. Teepe, E.R. Roux, S.D. Lyman, K. Shortman, and H.J. McKenna. 1996. Dramatic increase in the numbers of functionally mature dendritic cells in Flt3 ligand-treated mice: multiple dendritic cell subpopulations identified. *J. Exp. Med*. 184:1953–1962.
12. McKenna, H.J. 2000. Mice lacking Flt3 ligand have deficient hematopoiesis affecting hematopoietic progenitor cells, dendritic cells, and natural killer cells. *Blood*. 95:3489–3497.
13. D'Amico, A., and L. Wu. 2003. The early progenitors of mouse dendritic cells and plasmacytoid predendritic cells are within the bone marrow hemopoietic precursors expressing Flt3. *J. Exp. Med*. 198:293–303.
14. Brasel, K., H.J. McKenna, P.J. Morrissey, K. Charrier, A.E. Morris, C.C. Lee, D.E. Williams, and S.D. Lyman. 1996. Hematologic effects of flt3 ligand in vivo in mice. *Blood*. 88:2004–2012.
15. Wiktor-Jedrzejczak, W., E. Urbanowska, and M. Szperl. 1994. Granulocyte-macrophage colony-stimulating factor corrects macrophage deficiencies, but not osteopetrosis, in the colony-stimulating factor-1-deficient op/op mouse. *Endocrinology*. 134:1932–1935.
16. Dieu-Nosjean, M.C., A. Vicari, S. Lebecque, and C. Caux. 1999. Regulation of dendritic cell trafficking: a process that involves the participation of selective chemokines. *J. Leukoc. Biol*. 66:252–262.
17. Kurihara, T., G. Warr, J. Loy, and R. Bravo. 1997. Defects in macrophage recruitment and host defense in mice lacking the CCR2 chemokine receptor. *J. Exp. Med*. 186:1757–1762.
18. Kennedy, D.W., and J.L. Abkowitz. 1998. Mature monocytic cells enter tissues and engraft. *Proc. Natl. Acad. Sci. USA*. 95:14944–14949.
19. Inaba, K., M. Inaba, M. Deguchi, K. Hagi, R. Yasumizu, S. Ikehara, S. Muramatsu, and R.M. Steinman. 1993. Granulocytes, macrophages, and dendritic cells arise from a common major histocompatibility complex class II-negative progenitor in mouse bone marrow. *Proc. Natl. Acad. Sci. USA*. 90:3038–3042.
20. Manz, M.G., D. Traver, K. Akashi, M. Merad, T. Miyamoto, E.G. Engleman, and I.L. Weissman. 2001. Dendritic cell development from common myeloid progenitors. *Ann. N. Y. Acad. Sci*. 938:167–173 .
21. Akashi, K., D. Traver, T. Miyamoto, and I.L. Weissman. 2000. A clonogenic common myeloid progenitor that gives rise to all myeloid lineages. *Nature*. 404:193–197.
22. Fogg, D.K., C. Sibon, C. Miled, S. Jung, P. Aucouturier, D.R. Littman, A. Cumano, and F. Geissmann. 2006. A clonogenic bone marrow progenitor specific for macrophages and dendritic cells. *Science*. 311:83–87.
23. Varol, C., L. Landsman, D.K. Fogg, L. Greenshtein, B. Gildor, R. Margalit, V. Kalchenko, F. Geissmann, and S. Jung. 2007. Monocytes give rise to mucosal, but not splenic, conventional dendritic cells. *J. Exp. Med*. 204:171–180.
24. Naik, S.H., P. Sathe, H.Y. Park, D. Metcalf, A.I. Proietto, A. Dakic, S. Carotta, M. O'Keeffe, M. Bahlo, A. Papenfuss, et al. 2007. Development of plasmacytoid and conventional dendritic cell subtypes from single precursor cells derived in vitro and in vivo. *Nat. Immunol*. 8:1217–1226.
25. Onai, N., A. Obata-Onai, M.A. Schmid, T. Ohteki, D. Jarrossay, and M.G. Manz. 2007. Identification of clonogenic common Flt3(+)M-CSFR(+) plasmacytoid and conventional dendritic cell progenitors in mouse bone marrow. *Nat. Immunol*. 8:1207–1216.
26. Jose, M.D., Y. Le Meur, R.C. Atkins, and S.J. Chadban. 2003. Blockade of macrophage colony-stimulating factor reduces macrophage proliferation and accumulation in renal allograft rejection. *Am. J. Transplant*. 3:294–300.
27. Murayama, T., M. Yokode, H. Kataoka, T. Imabayashi, H. Yoshida, H. Sano, S. Nishikawa, S. Nishikawa, and T. Kita. 1999. Intraperitoneal administration of anti-c-fms monoclonal antibody prevents initial events of atherogenesis but does not reduce the size of advanced lesions in apolipoprotein E-deficient mice. *Circulation*. 99:1740–1746.
28. Sudo, T., S. Nishikawa, M. Ogawa, H. Kataoka, N. Ohno, A. Izawa, S. Hayashi, and S. Nishikawa. 1995. Functional hierarchy of c-kit and c-fms in intramarrow production of CFU-M. *Oncogene*. 11:2469–2476.
29. Geissmann, F., S. Jung, and D.R. Littman. 2003. Blood monocytes consist of two principal subsets with distinct migratory properties. *Immunity*. 19:71–82.
30. Miyamoto, A., T. Kunisada, H. Yamazaki, K. Miyake, S.I. Nishikawa, T. Sudo, L.D. Shultz, and S.I. Hayashi. 1998. Establishment and characterization of pro-B cell lines from motheaten mutant mouse defective in SHP-1 protein tyrosine phosphatase. *Immunol. Lett*. 63:75–82.
31. Kitaura, H., P. Zhou, H.J. Kim, D.V. Novack, F.P. Ross, and S.L. Teitelbaum. 2005. M-CSF mediates TNF-induced inflammatory osteolysis. *J. Clin. Invest*. 115:3418–3427.
32. Nahrendorf, M., F.K. Swirski, E. Aikawa, L. Stangenberg, T. Wurdinger, J.L. Figueiredo, P. Libby, R. Weissleder, and M.J. Pittet. 2007. The healing myocardium sequentially mobilizes two monocyte subsets with divergent and complementary functions. *J. Exp. Med*. 204:3037–3047.
33. Imai, T., K. Hieshima, C. Haskell, M. Baba, M. Nagira, M. Nishimura, M. Kakizaki, S. Takagi, H. Nomiyama, T.J. Schall, and O. Yoshie. 1997. Identification and molecular characterization of fractalkine receptor CX3CR1, which mediates both leukocyte migration and adhesion. *Cell*. 91:521–530.
34. Jung, S., J. Aliberti, P. Graemmel, M.J. Sunshine, G.W. Kreutzberg, A. Sher, and D.R. Littman. 2000. Analysis of fractalkine receptor CX(3)CR1 function by targeted deletion and green fluorescent protein reporter gene insertion. *Mol. Cell. Biol*. 20:4106–4114.
35. Cook, D.N., S.C. Chen, L.M. Sullivan, D.J. Manfra, M.T. Wiekowski, D.M. Prosser, G. Vassileva, and S.A. Lira. 2001. Generation and analysis of mice lacking the chemokine fractalkine. *Mol. Cell. Biol*. 21:3159–3165.
36. Lesnik, P., C.A. Haskell, and I.F. Charo. 2003. Decreased atherosclerosis in CX3CR1−/− mice reveals a role for fractalkine in atherogenesis. *J. Clin. Invest*. 111:333–340.
37. Kanazawa, N., T. Nakamura, K. Tashiro, M. Muramatsu, K. Morita, K. Yoneda, K. Inaba, S. Imamura, and T. Honjo. 1999. Fractalkine and macrophage-derived chemokine: T cell-attracting chemokines expressed in T cell area dendritic cells. *Eur. J. Immunol*. 29:1925–1932.
38. Ancuta, P., R. Rao, A. Moses, A. Mehle, S.K. Shaw, F.W. Luscinskas, and D. Gabuzda. 2003. Fractalkine preferentially mediates arrest and migration of $CD16^+$ monocytes. *J. Exp. Med*. 197:1701–1707.
39. Haskell, C.A., M.D. Cleary, and I.F. Charo. 2000. Unique role of the chemokine domain of fractalkine in cell capture. Kinetics of receptor dissociation correlate with cell adhesion. *J. Biol. Chem*. 275:34183–34189.
40. Fong, A.M., L.A. Robinson, D.A. Steeber, T.F. Tedder, O. Yoshie, T. Imai, and D.D. Patel. 1998. Fractalkine and CX_3CR1 mediate a novel mechanism of leukocyte capture, firm adhesion, and activation under physiologic flow. *J. Exp. Med*. 188:1413–1419.
41. Goda, S., T. Imai, O. Yoshie, O. Yoneda, H. Inoue, Y. Nagano, T. Okazaki, H. Imai, E.T. Bloom, N. Domae, and H. Umehara. 2000. CX3C-chemokine, fractalkine-enhanced adhesion of THP-1 cells to endothelial cells through integrin-dependent and -independent mechanisms. *J. Immunol*. 164:4313–4320.
42. Auffray, C., D. Fogg, M. Garfa, G. Elain, O. Join-Lambert, S. Kayal, S. Sarnacki, A. Cumano, G. Lauvau, and F. Geissmann. 2007. Monitoring of blood vessels and tissues by a population of monocytes with patrolling behavior. *Science*. 317:666–670.
43. Cardona, A.E., E.P. Pioro, M.E. Sasse, V. Kostenko, S.M. Cardona, I.M. Dijkstra, D. Huang, G. Kidd, S. Dombrowski, R. Dutta, et al. 2006. Control of microglial neurotoxicity by the fractalkine receptor. *Nat. Neurosci*. 9:917–924.
44. Serbina, N.V., W. Kuziel, R. Flavell, S. Akira, B. Rollins, and E.G. Pamer. 2003. Sequential MyD88-independent and -dependent activation of innate immune responses to intracellular bacterial infection. *Immunity*. 19:891–901.
45. Serbina, N.V., and E.G. Pamer. 2006. Monocyte emigration from bone marrow during bacterial infection requires signals mediated by chemokine receptor CCR2. *Nat. Immunol*. 7:311–317.
46. Serbina, N.V., T.P. Salazar-Mather, C.A. Biron, W.A. Kuziel, and E.G. Pamer. 2003. TNF/iNOS-producing dendritic cells mediate innate immune defense against bacterial infection. *Immunity*. 19:59–70.
47. Jakubzick, C., F. Tacke, F. Ginhoux, A.J. Wagers, N. van Rooijen, M. Mack, M. Merad, and G.J. Randolph. 2008. Blood monocyte subsets differentially give rise to CD103+ and CD103- pulmonary dendritic cell populations. *J. Immunol*. 180:3019–3027.

Published March 9, 2009

48. Brand, S., T. Sakaguchi, X. Gu, S.P. Colgan, and H.C. Reinecker. 2002. Fractalkine-mediated signals regulate cell-survival and immune-modulatory responses in intestinal epithelial cells. *Gastroenterology*. 122:166–177.
49. Shulby, S.A., N.G. Dolloff, M.E. Stearns, O. Meucci, and A. Fatatis. 2004. CX3CR1-fractalkine expression regulates cellular mechanisms involved in adhesion, migration, and survival of human prostate cancer cells. *Cancer Res*. 64:4693–4698.
50. Tsou, C.L., W. Peters, Y. Si, S. Slaymaker, A.M. Aslanian, S.P. Weisberg, M. Mack, and I.F. Charo. 2007. Critical roles for CCR2 and MCP-3 in monocyte mobilization from bone marrow and recruitment to inflammatory sites. *J. Clin. Invest*. 117:902–909.

SUPPLEMENTAL MATERIAL

Auffray et al., http://www.jem.org/cgi/content/full/jem.20081385/DC1

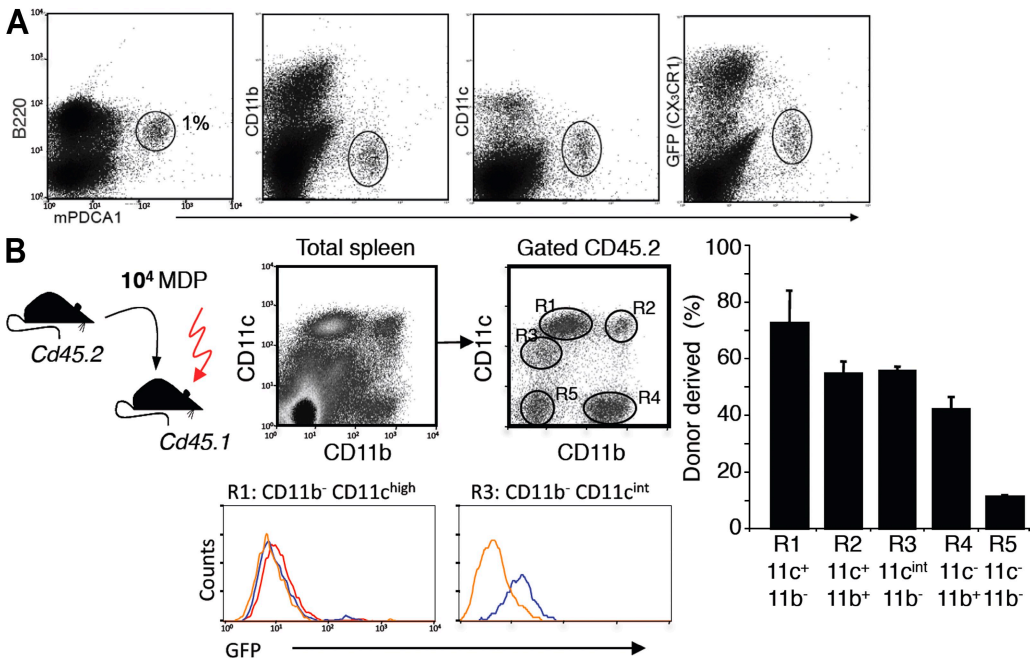

Figure S1. Expression of CX_3CR1 by PDCs. (A) PDCs express CX_3CR1. PDCA1$^+$ cells among $Cx_3cr1^{gfp/+}$ C57Bl/6 splenocytes express gfp/CX_3CR1 and intermediate levels of CD11c and B220. (B) Adoptive transfer of MDPs into irradiated host (900 rad). MDPs from Cd45.2 mice were adoptively transferred into Cd45.1 congenic recipients. Spleens of recipient mice were analysed at day 7 after transfer by flow cytometry using lineage marker and CD11b, CD11c, and CD8a$^+$ antibodies. The experiment was repeated five times with two to three mice per group and with similar results. Histograms represent the frequency of splenocytes derived from donor CD45.2 MDPs in an experiment with a high efficiency of MDP engraftment. Donor MDP appears to be very efficient at generating the population in R3 (CD11cint CD11b neg), which appears to be distinct from cDCs in R1 because they express lower CD11c and higher CX_3CR1. Error bars show SD.

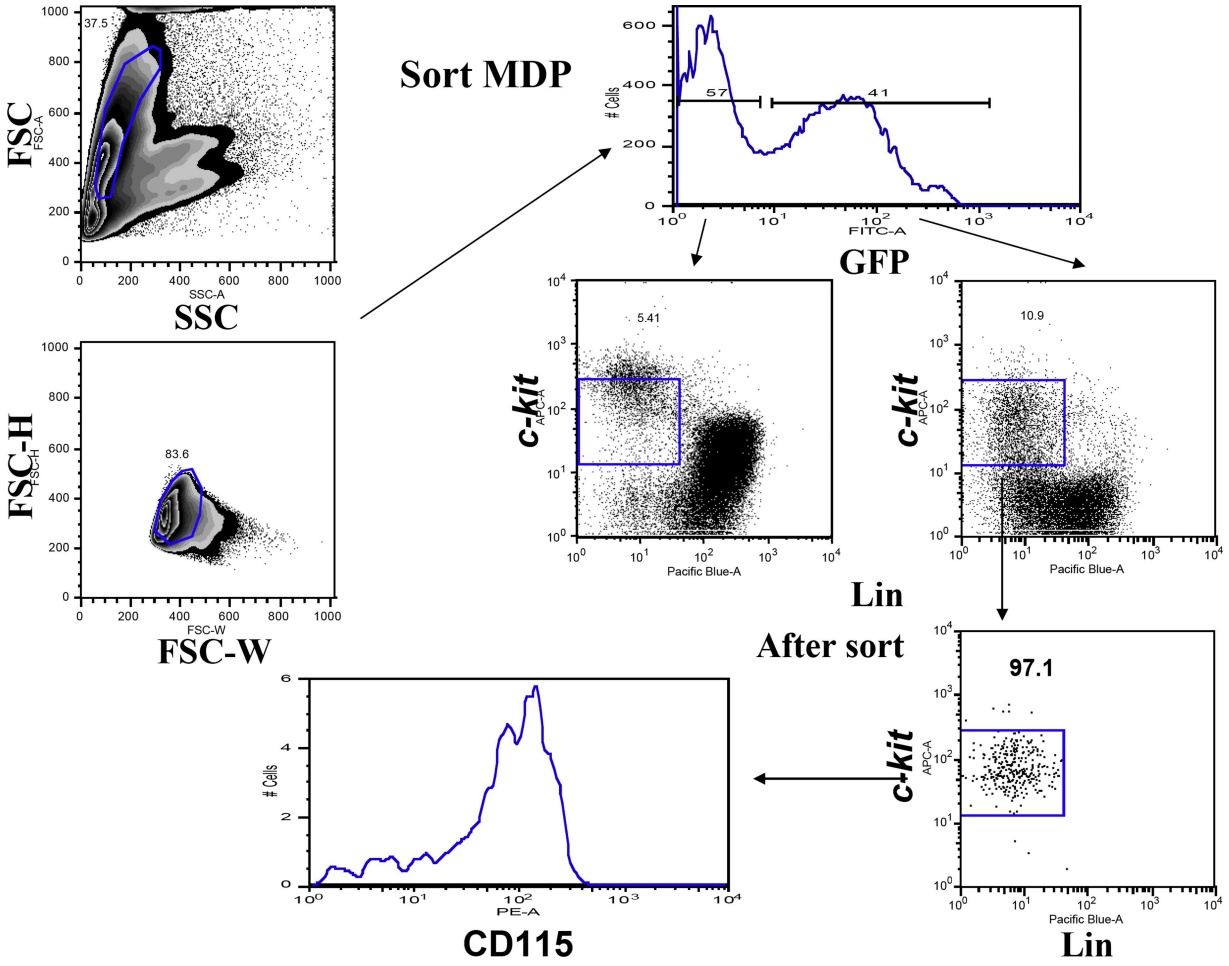

Figure S2. Sorting gates for MDPs and purity after sort.

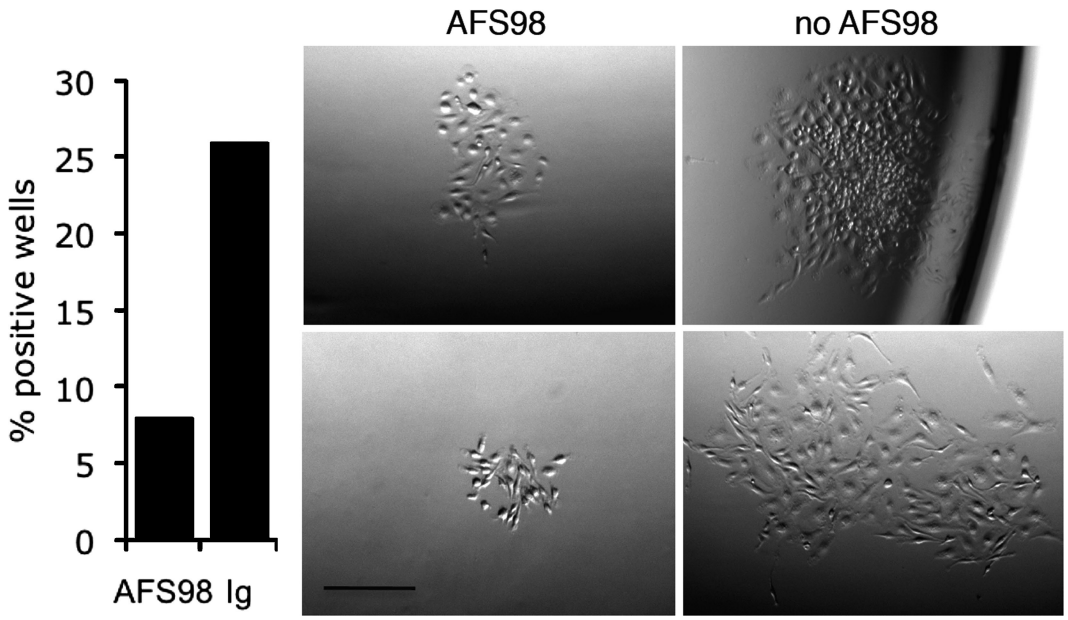

Figure S3. Effects of the AFS98 anti-CD115 antibody on the response of MDP to M-CSF in vitro. BM cells from *Cx$_3$cr1$^{gfp/+}$* mice were labeled with IL7Ra, CD117, a lineage cocktail (CD11c, CD11b, NK1.1, CD3, Ter119, CD19, and Gr1), antibodies, or with the same cocktail plus PE-conjugated anti-CD115 antibody (AFS98) at a 1/100 dilution. MDPs defined as lineage$^-$ CX$_3$CR1$^+$ CD117^{int-} were sorted as single cells with a FACSAria into 96-well plates and cultured in the presence of 50 ng/ml CSF-1 as previously described (Fogg, D.K., C. Sibon, C. Miled, S. Jung, P. Aucouturier, D.R. Littman, A. Cumano, and F. Geissmann. 2006. *Science*. 311:83–87). Positive wells were counted at day 7 (left) and photographed. Representative bright-field pictures of clones grown from single MDPs sorted with or without AFS98 in the antibody cocktail are displayed on the right. AFS98 was only added to the antibody cocktail for cell sorting, and no AFS98 was added during culture. Bar, 100 µm.

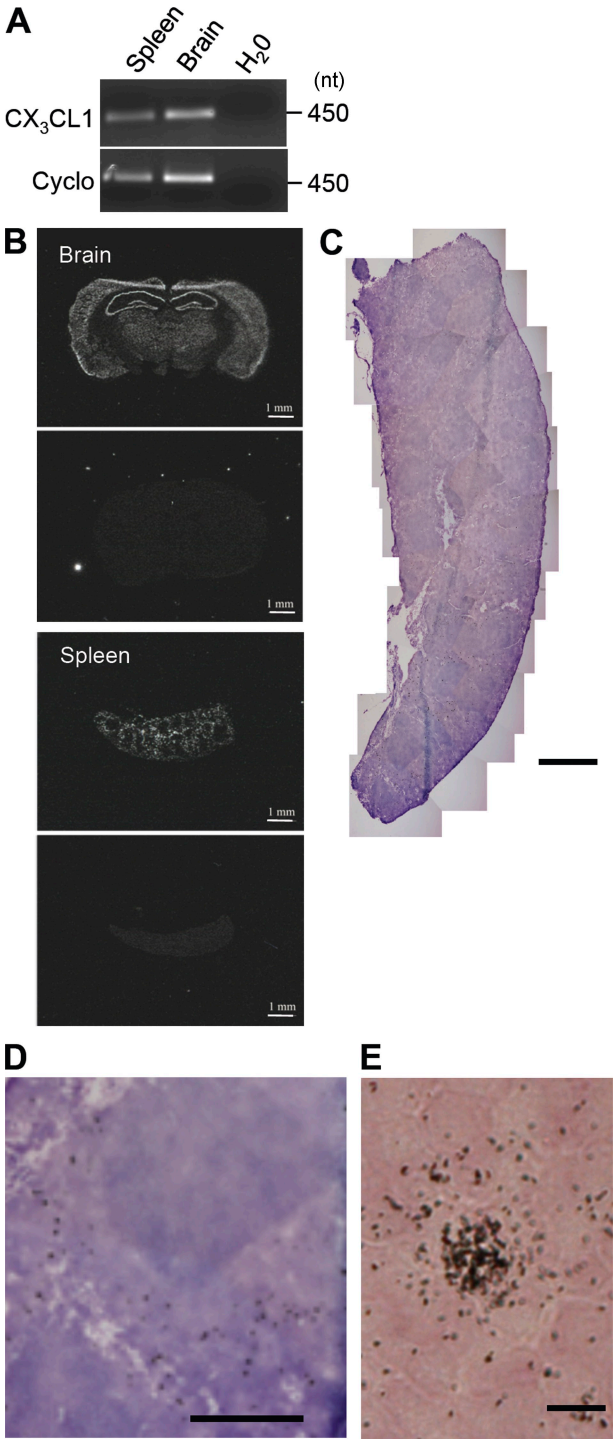

Figure S4. Fractalkine/CX_3CL1 expression and recruitment of monocytes to the spleen. (A) Mouse fractalkine/CX_3CL1 transcripts are detected in the spleen and brain of C57/Bl6 mice. Ubiquitously expressed cyclophilin (cyclo) is shown as a reference. (B) Expression of CX_3CL1 is detected in autoradiograms from brain tissue sections (positive control), and spleen tissue sections from WT mice, hybridized with antisense (top) and sense (negative control; bottom) ^{35}S-labeled probes are also detected. Bar, 1 mm. (C) Bright-field micrographs from spleen tissue section hybridized with the Cx_3cl1 antisense probe. CX_3CL1 transcript-positive cells were detected around B cell follicles, in the marginal zone/T cell area. Bar, 500 µm. (D) Magnification of C, making it possible to see the perifollicular locations of positive cells. Bar, 200 µm. (E) magnification of C to distinguish the numerous silver grain in the positive cells. Bar, 10 µm .

Cell Cycle (Data brut)	Bone marrow	Spleen n=6
% G1	58.8	95.33 ±1.12
% S	19.5	0.99 ±0.22
% G2/M	17.3	1.85 ±036

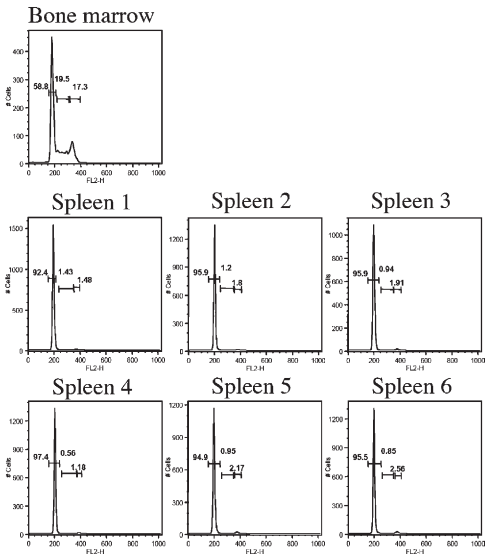

Figure S5. Analysis of the proliferation of monocytes in the spleen and BM. BALB/c mice were infected with 3×10^3 bacteria. 48 h later, spleen and leg bones were harvested. BM was flushed with RPMI 5% FCS and spleen were treated with collagenase/DNase. After lysis of red blood cells, cell suspensions were separately enriched for CD11b (MACs) and stained for CD11b, Ly6c, DX5, CD3, CD19, and Ly6G surface markers. Monocytes ($CD11b^+$ $Ly6C^+$ $DX5^-$ $CD3^-$ $CD19^-$ $Ly6G^-$) were sorted and splenic monocytes from individual mice were treated independently for cell cycle, whereas monocytes from BM were pooled. Cell cycle is defined as the following: cells were washed in PBS and fixed in 70% EtOH at 4°C for 30 minutes. Samples were then stained with 50 µg/ml PI in PBS complemented with 50 µg/ml RNase at 37°C for 30 min. Samples were then analyzed by flow cytometry.

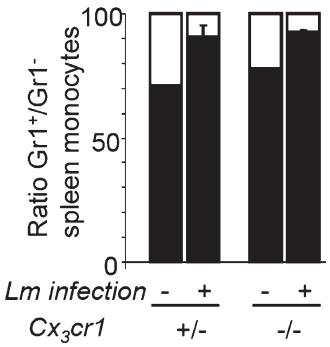

Figure S6. Ratio of $Gr1^+$ and $Gr1^-$ monocytes in the spleens of infected and control mice. BALB/c $Cx_3cr1^{+/-}$ and $Cx_3cr1^{-/-}$ were infected with 3×10^5 bacteria or received PBS as control. Bar graphs show the frequency (mean ± SEM) of spleen monocytes subsets in infected and controls mice. Error bars represent mean and SD (n = 4–6 mice per group).

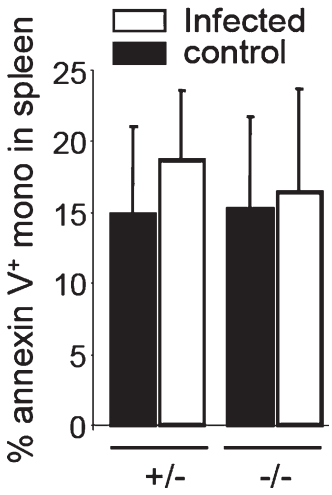

Figure S7. Frequency of annexin-V–positive cells in the spleens of infected and control mice. BALB/c $Cx_3cr1^{+/-}$ and $Cx_3cr1^{-/-}$ were infected with 3×10^5 bacteria or received PBS as control. Bar graphs show annexin-V binding by spleen monocytes after 24 h by flow cytometry in individual mice. Error bars represent mean and SD (n = 4–6 mice per group).

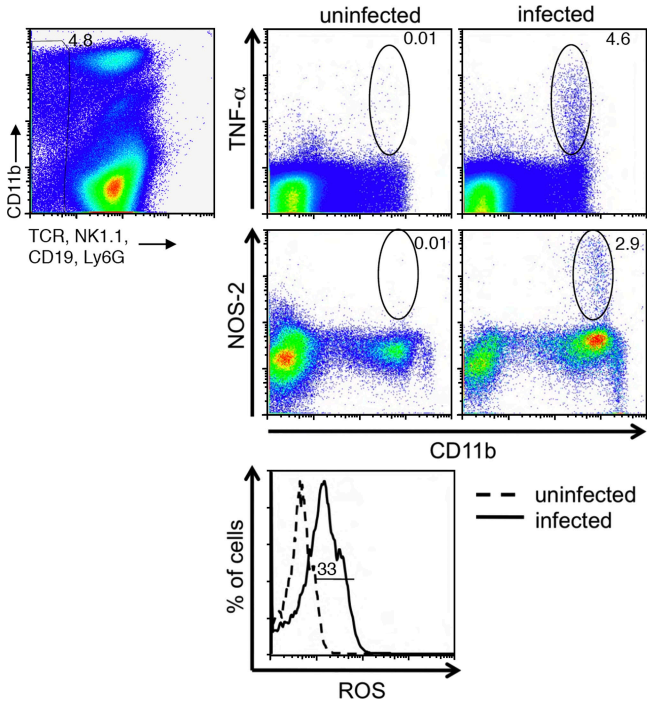

Figure S8. Production of TNF-α, iNOS, and ROI by lineage$^-$ CD11c^{low} CD11b$^+$ Gr1$^+$/Ly6c$^+$ spleen cells from uninfected C57/Bl6 mice and C57/Bl6 mice infected with 7×10^3 bacteria for 48 h.

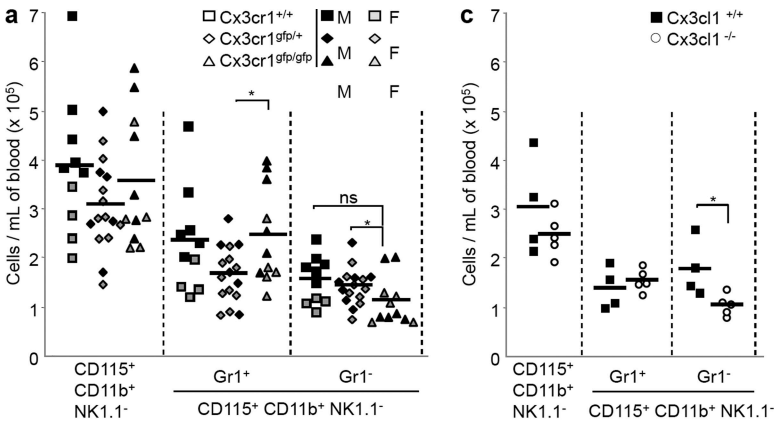

b

CD115+ CD11b+	Cx3cr1gfp/gfp	Cx3cr1+/+	Cx3cr1gfp/+
Cx3cr1gfp/gfp			
Cx3cr1+/+	0.5262		
Cx3cr1gfp/+	0.4897	0.1023	

Gr1+	Cx3cr1gfp/gfp	Cx3cr1+/+	Cx3cr1gfp/+
Cx3cr1gfp/gfp			
Cx3cr1+/+	0.7782		
Cx3cr1gfp/+	0.0484	0.0578	

Gr1-	Cx3cr1gfp/gfp	Cx3cr1+/+	Cx3cr1gfp/+
Cx3cr1gfp/gfp			
Cx3cr1+/+	0.0671		
Cx3cr1gfp/+	0.0382	0.5271	

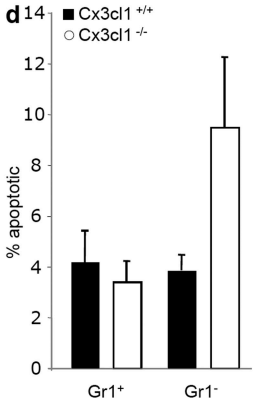

Figure S9. Monocyte survival in CX_3CR1-deficient mice and CX_3CL1-deficient mice. (a) Total blood monocytes ($CD115^+$ $CD11b^+$ $NK1.1^-$) and subsets ($Gr1^+/Ly6c^+$ and $Gr1^+/Ly6c^-$ monocytes) were enumerated in blood from *$Cx_3cr1^{+/+}$* (squares), *$Cx_3cr1^{gfp/+}$* (diamonds), and *$Cx_3cr1^{gfp/gfp}$* (triangles) 6–8-wk-old littermates. Each symbol corresponds to an individual mouse. Numbers for female mice are gray and for male mice are black. (b) The table represents p-values from the Wilcoxon test for the monocytes counts displayed in a. (c) Total blood monocytes ($CD115^+$ $CD11b^+$ $NK1.1^-$) and subsets ($Gr1^+/Ly6c^+$ and $Gr1^+/Ly6c^-$ monocytes) were enumerated in blood from *$Cx_3cl1^{+/+}$* (filled squares) and *$Cx_3cl1^{-/-}$* (open circles) mice. Horizontal lines represent the mean of results from individual mice. (d) Annexin-V staining of $Ly6c^+$ monocytes and $Ly6c^-$ monocytes in *$Cx_3cl1^{+/+}$* and *$Cx_3cL1^{-/-}$* mice. Asterisks indicate significative differences between groups ($P < 0.05$ using the Wilcoxon test). Error bars show SD.

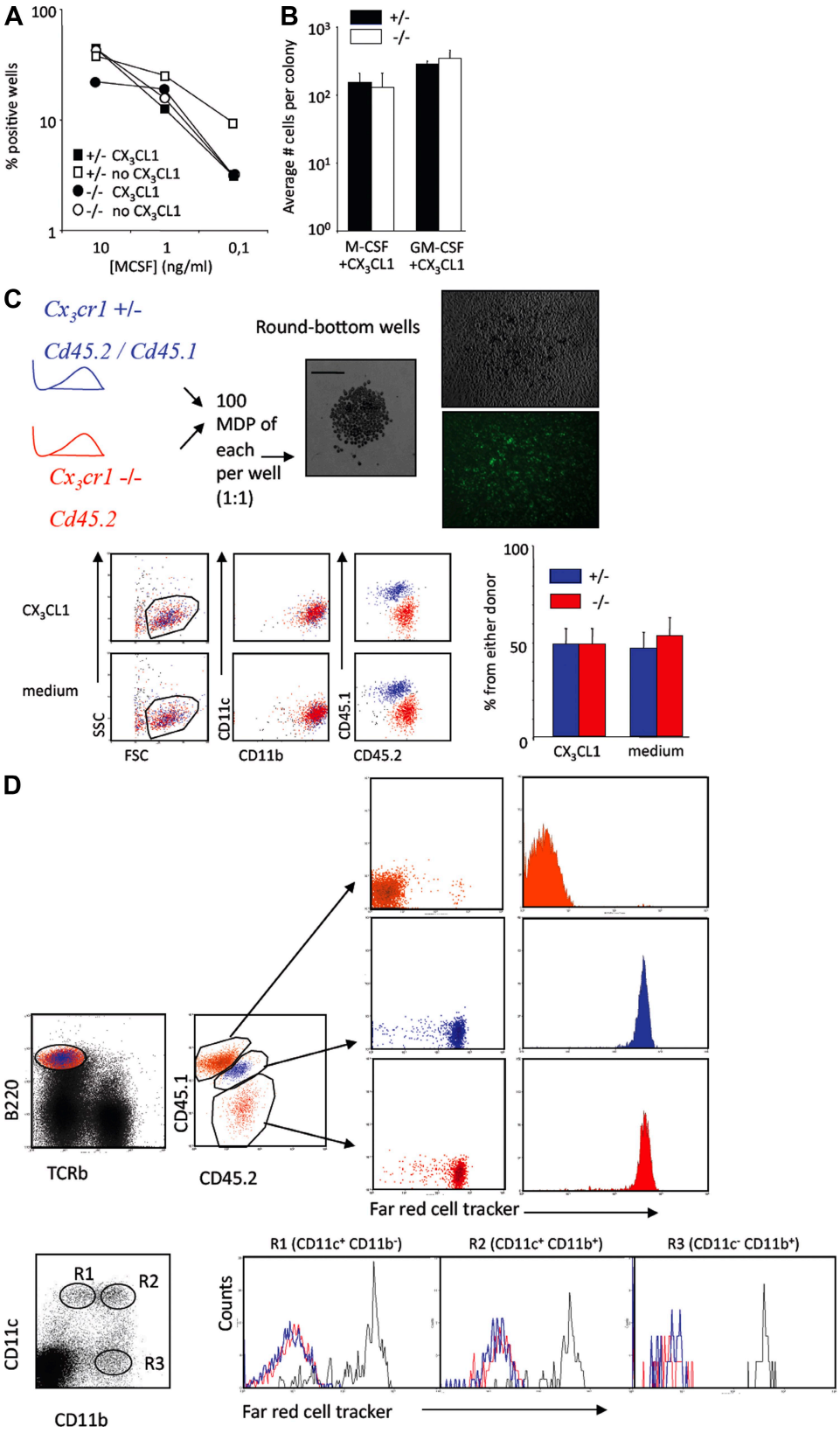

Figure S10. CX_3CR1 and CX_3CL1 are dispensable for MDP cloning, survival, and proliferation in vitro and in vivo. (a) In vitro cloning efficiency of MDPs. MDP from *$Cx_3cr1^{+/-}$* and *$Cx_3cr1^{-/-}$* mice were purified by flow cytometry as previously described (Fogg, D.K., C. Sibon, C. Miled, S. Jung, P. Aucouturier, D.R. Littman, A. Cumano, and F. Geissmann. 2006. *Science.* 311:83–87) and cloned in a 96-well plate coated with recombinant CX_3CL1-fractalkine or BSA alone and in the presence of increasing concentration of M-CSF. Cloning efficiency was measured as previously described (Fogg, D.K., C. Sibon, C. Miled, S. Jung, P. Aucouturier, D.R. Littman, A. Cumano, and F. Geissmann. 2006. *Science.* 311:83–87), and wells containing a colony of at least 200 cells after 3–10 d of culture were considered positive. The experiment was performed three times with similar results. (b) Proliferation of MDP. Bar graphs represent the mean size of colonies obtained from single clones described in a and for similar experiments in which M-CSF was replaced wth GM-CSF. Results are the mean and SD from three experiments. (c) In vitro competition experiment. Equal numbers (10^2) of MDP from *$Cx_3cr1^{+/-}$ Cd45.1/2* mice (blue) and *$Cx_3cr1^{-/-}$Cd45.2/2* mice (red) were mixed and seeded in round-bottom 96-well plates coated with recombinant CX_3CL1 or BSA alone and cultivated in culture medium with 10 ng/ml M-CSF. The percentages of CD45.1/2 and CD45.2/2 cells were determined after 5 d of culture. At least 10 wells were studied for each experimental condition. The bar graph represents the mean and SD of a representative experiment out of four experiments performed. Bar, 100 µm. (d) In vivo proliferation of MDPs and MDP-derived cells. 10^4 MDPs from *$Cx_3cr1^{+/-}$ Cd45.1/2* mice (blue), 10^4 MDPs from *$Cx_3cr1^{-/-}$ Cd45.2/2* mice (red), and 10^6 $CD19^+$ B cells (as a control; black) were labeled with Cell Tracker 633 (Bodipy 630/650 MeBr) and adoptively transferred into an irradiated (1,000 rad) *Cd45.1* congenic recipient. 6 d later, donor MDP-derived cells from both *Cd45.1/2* and *Cd45.2/2* mice were no longer labeled, whereas B cells retained the dye.